conversions. The strongly adsorbed alkyl species, however, did appear to participate in the formation of products. The extension of the various NMR techniques to allow data accumulation at low temperatures will help uncover the operable mechanism in the adsorption and reaction of ethylene on silica-supported ruthenium.

V. Conclusions

NMR allows detection of chemisorbed species and also weakly adsorbed molecules at coverages higher than those used in spectroscopies employing ultrahigh vacuum conditions. The application of ^{13}C high-resolution NMR techniques allows the formation of a coherent picture of the chemistry of a relatively complex system by determining the structure and abundance of molecular species adsorbed on the catalyst surface. The ^{13}C CP/MAS technique allows simultaneous observation of the transformations of chemisorbed and weakly adsorbed molecules. Direct ^{13}C excitation allows quantitative measurements of the various species present.

From these experiments we observed the decomposition of ethylene at room temperature to form strongly adsorbed species identified as acetylide and alkyl groups. Recombination of the adsorbed alkyl species and hydrogenation of ethylene occurred rapidly at room temperature and formed weakly adsorbed ethane and *cis*- and *trans*-2-butene that subsequently hydrogenated to butane. The formation of C–C bonds is postulated to take place through a metallocycle adsorbed species.

The strongly adsorbed species identified as acetylide was not appreciably consumed in the formation of products, although it may have served as a host for other reactions. Finally, spin counting revealed that there was one carbon in the strongly adsorbed layer for each surface ruthenium atom.

Acknowledgment. This work was supported by the U.S. Department of Energy, Office of Basic Energy Sciences, Contract Number W-7405-ENG-82. One of the authors (J.C.K.) acknowledges the financial support of the Amoco foundation. Additional support was obtained from the Iowa State University Engineering Research Institute.

Registry No. $H_2C{=}CH_2$, 74-85-1; Ru, 7440-18-8; CH_3CH_3, 74-84-0; $CH_3(CH_2)_2CH_3$, 106-97-8; *trans*-butene, 624-64-6; *cis*-butene, 590-18-1.

Light Noble Gas Chemistry: Structures, Stabilities, and Bonding of Helium, Neon and Argon Compounds

Gernot Frenking,*,†,[1a] Wolfram Koch,[1b] Felix Reichel,[1c] and Dieter Cremer*,[1d]

Contribution from the Institut für Organische Chemie, Universität Marburg, Hans-Meerwein-Strasse, D-3550 Marburg, West Germany, the Institute for Superconducting and Applied Mathematics, IBM Scientific Center, Tiergartenstrasse 15, D-6900 Heidelberg, West Germany, the Institut für Organische Chemie, Universität Köln, Greinstrasse 4, D-5000 Köln 41, West Germany, and Theoretical Chemistry, University of Göteborg, Kemigårde 3, S-41296 Göteborg, Sweden. *Received July 10, 1989*

Abstract: Theoretically determined geometries are reported for the light noble gas ions Ng_2C^{2+}, Ng_2N^{2+}, Ng_2O^{2+}, $NgCCNg^{2+}$, $NgCCH^+$, $NgCN^+$, and $NgNC^+$ (Ng = He, Ne, Ar) at the MP2/6-31G(d,p) level of theory. In a few cases, optimizations were carried out at CASSCF/6-31G(d,p). The thermodynamic stability of the Ng compounds is investigated at MP4(SDTQ)/6-311G(2df,2pd) for Ng = He, Ne and at MP4(SDTQ)/6-311G(d,p) for Ng = Ar. The structures and stabilities of the molecules are discussed in terms of donor–acceptor interactions between Ng and the respective fragment cation, by using molecular orbital arguments and utilizing the analysis of the electron density distribution and its associated Laplace field. Generally, there is an increase in Ng,X binding interactions of a noble gas molecule NgX with increasing atomic size of Ng. In some cases the Ne,X stabilization energies are slightly smaller than the corresponding He,X values because of repulsive p–π interactions in the neon compounds. The argon molecules are in all cases significantly stronger bound.

1. Introduction

In a recent theoretical study of compounds containing the most inert chemical element helium, we found[2] that He can form strong chemical bonds in ions and may even be bound in the ground state of a neutral molecule, i.e., HeBeO. The most important criterion for a potential binding partner of helium is its electronic structure, rather than its electronegativity or positive charge. The structures and stabilities of He compounds could be rationalized by using the model of a donor–acceptor complex.[2] Helium bonds can be very strong with a dissociation energy of up to 90 kcal/mol, if the binding partner provides low-lying empty σ orbitals. The electronic structure of the molecules has been investigated with the aid of an electron density analysis. This revealed covalent He,C bonds in several cations and dications.[2] The neutral compound HeBeO was found, however, to be an unusually stable (D_0 = 3 kcal/mol) van der Waals complex where the attractive interactions are dominated by charge-induced dipole interactions.[2,3]

There are two other noble gas elements, neon and argon, which have resisted so far all attempts to force them into binding with other atoms to form a stable compound.[4] Little is known about neon and argon chemistry.[5] In two recent papers we have investigated the electronic structure and bonding in diatomic cations HeX^+,[6] NeX^+, and ArX^+[7] with X being a first-row element

† Part of this work was performed at the Molecular Research Institute, Palo Alto, CA.

(1) (a) Universität Marburg. (b) IBM Scientific Center. (c) Universität Köln. (d) University of Göteborg.

(2) Koch, W.; Frenking, G.; Gauss, J.; Cremer, D.; Collins, J. R. *J. Am. Chem. Soc.* **1987**, *109*, 5917.

(3) Frenking, G.; Koch, W.; Gauss, J.; Cremer, D. *J. Am. Chem. Soc.* **1988**, *110*, 8007.

(4) Weakly bound neutral van der Waals complexes and clathrates containing noble gas elements are known for many years. See ref 5 and Holloway, J. H. *Noble-Gas Chemistry*; Methuen, London, 1968.

(5) Frenking, G.; Cremer, D. In *Structure and Bonding*; Springer: Heidelberg, 1990; Vol. 73.

(6) Frenking, G.; Koch, W.; Gauss, J.; Cremer, D.; Liebmann, J. F. *J. Phys. Chem.* **1989**, *93*, 3397.

(7) Frenking, G.; Koch, W.; Gauss, J.; Cremer, D.; Liebmann, J. F. *J. Phys. Chem.* **1989**, *93*, 3410.

0002-7863/90/1512-4240$02.50/0

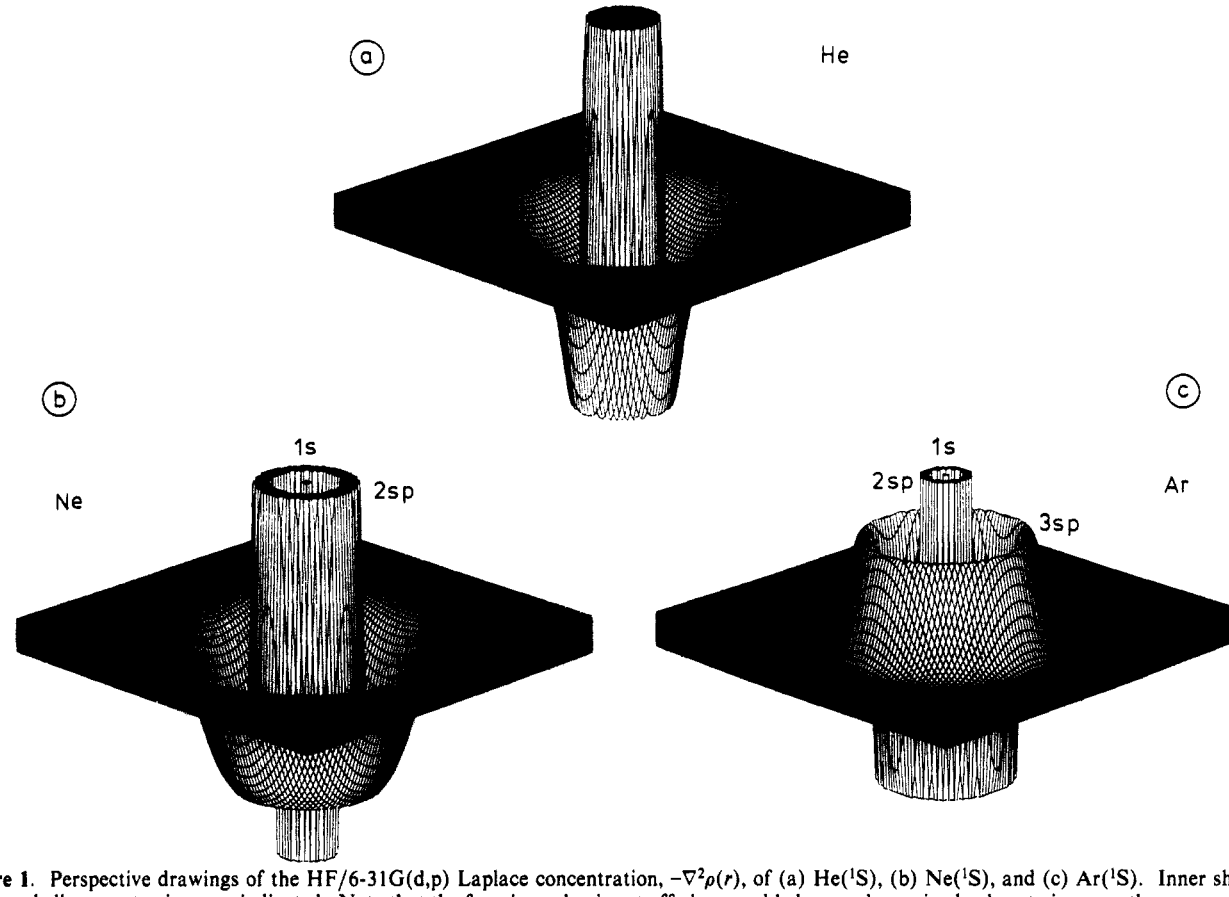

Figure 1. Perspective drawings of the HF/6-31G(d,p) Laplace concentration, $-\nabla^2\rho(r)$, of (a) He(^{1}S), (b) Ne(^{1}S), and (c) Ar(^{1}S). Inner shell and valence shell concentrations are indicated. Note that the function value is cut off above and below predetermined values to improve the representation.

Li–Ne. The electronic ground states of the diatomic ions are in most cases weakly bound van der Waals complexes held together by charge-induced dipole interactions, although in some cases covalent bonding has been predicted on the basis of an electron density analysis.[7] In particular, ($X^1\Sigma^+$) ArF^+ has been calculated with a dissociation energy D_0 of 49 ± 3 kcal/mol[7,8] which might be sufficient to form a stable salt compound.[8] Most of the excited states of NgX^+ have been predicted to be covalently bound.[6,7]

In this paper we extend our previous investigation of He compounds[2] to the heavier elements Ne and Ar. We discuss calculated results for NgX molecules which in the case of Ng = He were found[2] to be strongly bound. We present a systematic comparison of analogous helium, neon, and argon compounds based on ab initio calculations and the analysis of the electron density distribution of the computed molecular structures. The principle questions which we address are the following.

(a) Are there thermodynamically stable He, Ne, and Ar compounds? (b) What are the differences for a given structure NgX when Ng is either He, Ne, or Ar? (c) What are the stabilities of Ne and Ar compounds compared to those of He molecules? (d) Is the model of donor–acceptor interactions as valid for explaining neon and argon structures as it is for helium compounds? (e) How important are π-interactions in Ne and Ar structures?

We will answer these questions by analyzing energies, geometries, wave functions, i.e., MOs, and the total electron density distribution by using techniques that have been very useful in the theoretical investigation of noble gas compounds.[2,3,6,7]

2. Quantum Chemical Methods

A major part of our theoretical results has been obtained using the CRAY and IBM versions of GAUSSIAN 82[11a] and GAUSSIAN 86,[11b] respectively, and the program COLOGNE.[12] As a standard, molecular geometries have been optimized both at the Hartree–Fock (HF) and the second-order Møller–Plesset (MP2) perturbation[13] level employing the 6-31G(d,p) basis set. These levels of theory are denoted by HF/6-31G(d,p) and MP2/6-31G(d,p). Unless otherwise noted, all structures reported here have been verified as true minima on the potential energy surface with only positive eigenvalues of the force-constant matrix. Geometry optimizations were carried out by using analytical gradients. Harmonic vibrational frequencies and zero-point energies (ZPE) are determined at MP2/6-31G(d,p) and, in some cases, at HF/6-31G(d,p). The ZPE values have been scaled uniformly by a factor of 0.87 and 0.93 for the two levels of theory used.[14] Utilizing the geometries obtained at MP2/6-31G(d,p), single-point energies are calculated with a larger basis set and fourth-order Møller–Plesset perturbation theory.[13] For the argon compounds, the theoretical level is MP4(SDTQ)/6-311G(d,p) and for the helium and neon species it is MP4(SDTQ)/6-311G(2df,2pd). Unless otherwise specified, energy values in the text are given at these theoretical levels. For a few structures, CASSCF[15] calculations have been carried out with a full-valence active space and a 6-31G(d,p) basis set by using the program GAMESS.[16] The geometries have been obtained at

(8) Frenking, G.; Koch, W.; Deakyne, C.; Liebmann, J. F.; Bartlett, N. *J. Am. Chem. Soc.* **1989**, *111*, 31.
(9) Moore, C. E. *Analyses of Optical Spectra*; National Bureau of Standards, NSRDS-NBS 34; Washington, D.C., 1970.
(10) Miller, T. M.; Bederson, B. *Adv. At. Mol. Phys.* **1977**, *13*, 1.

(11) (a) Binkley, J. S.; Frisch, M. J.; DeFrees, D. J.; Raghavachari, K.; Whiteside, R. A.; Schlegel, H. B.; Fluder, E. M.; Pople, J. A. GAUSSIAN 82; Carnegie-Mellon University: Pittsburgh, PA. (b) Frisch, M. J.; Binkley, J. S.; Schlegel, H. B.; Raghavachari, K.; Melius, C. F.; Martin, R. L.; Sewart, J. J. P.; Bobrowicz, F. W.; Rohlfing, C. M.; Kahn, L. R.; DeFrees, D. J.; Seeger, R.; Whiteside, R. A.; Fox, D. J.; Fluder, E. M.; Pople, J. A. Carnegie-Mellon Quantum Chemistry Publishing Unit: Pittsburgh, PA, 1964.
(12) Gauss, J.; Kraka, E.; Reichel, F.; Cremer, D. COLOGNE 88; Universität Köln, 1988.
(13) (a) Møller, C.; Plesset, M. S. *Phys. Rev.* **1934**, *46*, 618. (b) Binkley, J. S.; Pople, J. A. *Int. J. Quantum Chem.* **1975**, *9S*, 229.
(14) Hout, R. F.; Levi, B. A.; Hehre, W. J. *J. Comput. Chem.* **1982**, *3*, 234.
(15) Roos, B. O. In *Ab Initio Methods in Quantum Chemistry*; Lawley, K. P.; Ed.; Wiley: New York, 1987; Vol. II.
(16) (a) Guest, M. F.; Kendrick, J.; Pope, S. A. GAMES Documentation; SERC Daresbury Laboratory: Daresbury, Warrington, WA4 4AD, 1983. (b) Dupuis, M.; Spangler, D.; Wendolowski, J. J. NRCC Software Catalog; 1980; Vol. 1, Program No. QG01. (c) The GAMESS version used was provided by the following: Schmidt, M.; Elbert, S. installed at San Diego Super Computer Center.

Table I. Some Properties of the Noble Gas Elements He, Ne, and Ar

property[a]	He(^{1}S)	Ne(^{1}S)	Ar(^{1}S)	ref
IP [eV]	24.59	21.56	15.6	9
α [Å^3]	0.205	0.395	1.64	10
χ	4.53	3.98	2.91	29
r_1 [Å]	0.34	0.46	0.93	this work
$\nabla^2\rho(r_1)$ [e/Å^5]	24.9	50.1	5.0	this work
r_2 [Å]		0.26	0.57	this work
$\nabla^2\rho(r_2)$ [e/Å^5]		−460	−29.2	this work
property[a]	He$^+$(^{2}S)	Ne$^+$(^{2}P)[b]	Ar$^+$(^{2}P)[b]	
r_1 [Å]	0.33	0.42	0.86	this work
$\nabla^2\rho(r_1)$ [e/Å^5]	25.1	84.2	6.4	this work
r_2 [Å]		0.25	0.55	this work
$\nabla^2\rho(r_2)$ [e/Å^5]		−752	−42.1	this work

[a] IP, α, and χ, denote ionization potential, electric polarizability, and electronegativity, respectively; r_1 and r_2 denote the radius of the valence shell concentration sphere and the valence shell depletion sphere, respectively (see Figure 1). They are measures for the size of an atom or ion. The corresponding values of the Laplace distribution are indicated by $\nabla^2\rho(r_i)$. [b] Laplace concentrations are anisotropic. Only values in the direction of the valence shell concentration maxima are given.

the CASSCF/6-31G(d,p) level by using analytical gradients.

The total electron density distribution $\rho(r)$ and its associated Laplace field $\nabla^2\rho(r)$ have been analyzed for the calculated structures in the same way as it was done in our previous study of helium compounds.[2] Details of the method and further examples of the application may be found in the literature.[17-26]

3. Results and Discussion

In Table I, some of the known properties of the three noble gas elements He, Ne, and Ar are summarized. The observed ionization potentials IP[9] and polarizabilities α[10] clearly show that both the donor ability and capability of interacting electrostatically with other elements increase from He to Ne and Ar. This is also reflected by the electronegativities χ that have been suggested for the three Ng elements by various authors.[29] All these data suggest that He, Ne, and Ar should be the most difficult elements to bind.

Figure 1 depicts perspective drawings of the HF/6-31G(d,p) Laplace concentrations of He, Ne, and Ar. The He atom possesses a single concentration peak surrounded by a sphere of depletion of negative charge (Figure 1a). For Ne (Figure 1b), two concentration and two depletion spheres can be distinguished. The inner concentration sphere is at the nucleus, while the outer concentration sphere is about in the valence region. It is appealing to associate the inner shell with the 1s electrons and the outer concentration shell with the valence electrons of Ne. Similarly one can speak of an inner shell depletion sphere and a valence shell depletion sphere.

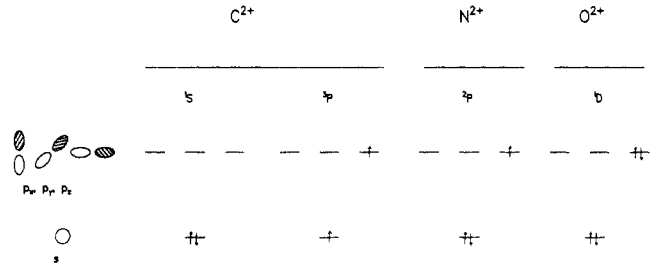

Figure 2. Schematic representation of the orbital occupance of C^{2+}, N^{2+}, and O^{2+}. Only one resonance structure for the p-electrons of the ^{1}D state of O^{2+} is shown.

For Ar (Figure 1c), three pairs of spheres with concentration or depletion of negative charge exist in the Laplace concentration $-\nabla^2\rho(r)$: The most inner can be associated with the 1s electrons of Ar, the next with the 2s2p electrons, and the most outer with the valence electrons of Ar. In Table I, calculated radii, r_i (r_1, valence depletion sphere; r_2, valence concentration sphere), and concentration values, $-\nabla^2\rho(r_i)$, for the three noble gas atoms are given.

Investigation of the concentration spheres of the atoms of the same period in the periodic table reveals that there is a direct relation between the degree of charge concentration and charge depletion in the valence shell. For example, the more electronegative an atom is, the smaller are the radii, r_i, of the valence spheres and the higher is the concentration of negative charge in the valence region. With the contraction of the valence sphere the outer depletion sphere becomes more pronounced and much deeper. It seems as if negative charge residing further away from the nucleus is pulled into the valence concentration sphere to increase electron-nucleus attraction and to leave an electron hole surrounding the valence sphere. The extent of charge concentration and the extent of charge depletion are indeed related as becomes immediately obvious from the local virial theorem[17]

$$\frac{1}{4}\nabla^2\rho(r) = 2G(r) + V(r)$$

which states that the kinetic energy density $G(r)$ and the potential energy density $V(r)$ add up at each point r in space to the Laplace distribution. Since integration over the total space must yield the virial theorem

$$\frac{1}{4}\int \nabla^2\rho(r)dr = 2\int G(r)dr + \int V(r)dr = 2T + V = 0$$

it follows that fluctuations in the Laplace distribution summed over all space vanish. The more the negative charge is concentrated in the valence shell, the deeper the surrounding depletion sphere. This can be seen for He and for Ne, where in the latter case the extension of the valence shell from two s electrons to additional six 2p electrons has a distinct effect on charge concentration and charge depletion in the valence shell (Table I and Figure 1a,b).

For Ar, the 2sp shell shields to some extent the nucleus. As a consequence, the 3sp valence shell is less contracted as can be seen for the Laplace concentration shown in Figure 1c. Also, the outer depletion sphere is rather shallow and less pronounced than that of Ne in accordance with the lower electronegativity of Ar (Table I). He and Ne are more related than Ne and Ar since the former atoms both possess deep valence shell depletion spheres while Ar does not.

3.1. Ng_2X^{2+} (X = C, N, O). The calculated energies of the Ng_2X^{2+} molecules **1S–9** are shown in Table II. Predicted reaction energies ΔE_e and ΔE_0 for some fragmentation reactions are listed in Scheme I, where subscripts e and o denote values at 0 K without and with ZPE correction. The optimized geometries are exhibited in Chart I.

Ions Ng_2C^{2+} are valence isoelectronic with methylene, CH_2. Contrary to CH_2, the calculated total energies of the methylene analogues Ng_2C^{2+} **1S–3T** shown in Table II indicate that the $^1A_1$ singlet state is lower in energy than the $^3B_1$ triplet state for Ng = He, Ne, and Ar. The energy differences are 63.8 kcal/mol (Ng

(17) Bader, R. F. W.; Nguyen-Dang, T. T.; Tal, Y. *Rep. Prog. Phys.* **1981**, *44*, 893.
(18) (a) Bader, R. F. W.; Slee, T. S.; Cremer, D.; Kraka, E. *J. Am. Chem. Soc.* **1983**, *105*, 5061. (b) Cremer, D.; Kraka, E.; Slee, T. S.; Bader, R. F. W.; Lau, C. D. H.; Nguyen-Dang, T. T.; MacDougall, P. J. *J. Am. Chem. Soc.* **1983**, *105*, 5069.
(19) (a) Cremer, D.; Kraka, E. In *Conceptual Approaches in Quantum Chemistry—Models and Applications*; Croat. *Chem. Acta* **1984**, *57*, 1259. (b) Cremer, D. In *Modelling of Structure and Properties of Molecules*; Maksic, Z. B., Ed.; Ellis Horwood: Chichester, 1987; p 87.
(20) Cremer, D.; Kraka, E. *Angew. Chem.* **1984**, *96*, 612; *Angew. Chem., Int. Ed. Engl.* **1984**, *23*, 627.
(21) (a) Cremer, D.; Kraka, E. *J. Am. Chem. Soc.* **1985**, *107*, 3800, 3811. (b) Cremer, D.; Kraka, E. In *Molecular Structure and Energetics*; Greenberg, A., Liebmann, J. F., Eds.; VCH Publishers: New York, Vol. 7, In press.
(22) Cremer, D.; Gauss, J. *J. Am. Chem. Soc.* **1986**, *108*, 7467.
(23) Koch, W.; Frenking, G.; Gauss, J.; Cremer, D.; Sawaryn, A.; Schleyer, P. v. R. *J. Am. Chem. Soc.* **1986**, *108*, 5732.
(24) Cremer, D.; Gauss, J.; Kraka, E. *J. Mol. Struct. THEOCHEM* **1988**, *169*, 531.
(25) (a) Bader, R. F. W.; MacDougall, P. J.; Lau, C. D. H. *J. Am. Chem. Soc.* **1984**, *106*, 1594. (b) Bader, R. F. W.; Essen, H. *J. Chem. Phys.* **1984**, *80*, 1943.
(26) Koch, W.; Frenking, G.; Gauss, J.; Cremer, D. *J. Am. Chem. Soc.* **1986**, *108*, 5808.

Scheme I. Calculated Fragmentation Energies (ΔE_e and ΔE_o, kcal/mol) at MP4(SDTQ)/6-311G(2df,2pd)//MP2/6-31G(d,p) (Helium and Neon Structures) MP4(SDTQ)/6-311G(d,p)//MP2/6-31(d,p) (Argon Structures)

reaction	ΔE_e	ΔE_o	no.
$He_2C^{2+}(^1A_1) \rightarrow C^{2+}(^1S) + 2He(^1S)$	+32.6	+30.6	1a
$He_2C^{2+}(^1A_1) \rightarrow C^{+}(^2P) + He^{+}(^2S) + He(^1S)$	+37.4	+35.4	1b
$He_2C^{2+}(^1A_1) \rightarrow HeC^{2+}(^1\Sigma^+) + He(^1S)$	+14.7	+13.6	1c
$HeC^{2+}(^1\Sigma^+) \rightarrow C^{2+}(^1S) + He(^1S)$	+17.9	+17.0	1d
$He_2C^{2+}(^3B_1) \rightarrow C^{2+}(^1S) + 2He(^1S)$	+117.4	+112.5	2a
$He_2C^{2+}(^3B_1) \rightarrow C^{+}(^2P) + He^{+}(^2S) + He(^1S)$	−23.4	−28.3	2b
$He_2C^{2+}(^3B_1) \rightarrow HeC^{2+}(^3\Pi) + He(^1S)$	+50.1	+47.2	2c
$HeC^{2+}(^3\Pi) \rightarrow C^{2+}(^3P) + He(^1S)$	+67.3	+65.3	2d
$Ne_2C^{2+}(^1A_1) \rightarrow C^{2+}(^1S) + 2Ne(^1S)$	+71.9	+70.6	3a
$Ne_2C^{2+}(^1A_1) \rightarrow C^{+}(^2P) + Ne^{+}(^2P) + Ne(^1S)$	+3.9	+2.6	3b
$Ne_2C^{2+}(^1A_1) \rightarrow NeC^{2+}(^1\Sigma^+) + Ne(^1S)$	+27.4	+27.0	3c
$NeC^{2+}(^1\Sigma^+) \rightarrow C^{2+}(^1S) + Ne(^1S)$	+44.5	+43.6	3d
$Ne_2C^{2+}(^3B_1) \rightarrow C^{2+}(^3P) + 2Ne(^1S)$	+143.0	+140.8	4a
$Ne_2C^{2+}(^3B_1) \rightarrow C^{+}(^2P) + Ne^{+}(^2P) + Ne(^1S)$	−70.7	−72.9	4b
$Ne_2(C^{2+}(^3B_1) \rightarrow NeC^{2+}(^3\Pi) + Ne(^1S)$	+53.6	+52.6	4c
$NeC^{2+}(^3\Pi) \rightarrow C^{2+}(^3P) + Ne(^1S)$	+89.4	+88.2	4d
$Ar_2C^{2+}(^1A_1) \rightarrow C^{2+}(^1S) + 2Ar(^1S)$	+178.6	+177.2	5a
$Ar_2C^{2+}(^1A_1) \rightarrow C^{+}(^2P) + Ar^{+}(^2P) + Ar(^1S)$	−26.7	−28.1	5b
$Ar_2(C^{2+}(^1A_1) \rightarrow ArC^{2+}(^1\Sigma^+) + Ar(^1S)$	+49.2	+48.8	5c
$ArC^{2+} \rightarrow C^{2+}(^1S) + Ar(^1S)$	+129.4	+128.4	5d
$Ar_2C^{2+}(^3B_1) \rightarrow C^{2+}(^3P) + 2Ar(^1S)$	+294.5	+292.3	6a
$Ar_2C^{2+}(^3B_1) \rightarrow C^{+}(^2P) + Ar^{+}(^2P) + Ar(^1S)$	−56.9	−59.1	6b
$Ar_2C^{2+}(^3B_1) \rightarrow ArC^{2+}(^3\Pi) + Ar(^1S)$	+89.2	+88.1	6c
$ArC^{2+} \rightarrow C^{2+}(^3P) + Ar(^1S)$	+205.3	+204.2	6d
$He_2N^{2+}(^2B_1) \rightarrow N^{2+}(^2P) + 2He(^1S)$	+86.2	+82.4	7a
$He_2N^{2+}(^2B_1) \rightarrow N^{+}(^3P) + He^{+}(^2S) + He(^1S)$	−30.4	−34.0	7b
$Ne_2N^{2+}(^2B_1) \rightarrow N^{2+}(^2P) + 2Ne(^1S)$	+133.4	+131.1	8a
$Ne_2N^{2+}(^2B_1) \rightarrow N^{+}(^3P) + Ne^{+}(^2P) + Ne(^1S)$	−55.9	−58.2	8b
$Ar_2N^{2+}(^2B_1) \rightarrow N^{2+}(^2P) + 2Ar(^1S)$	+276.4	+272.8	9a
$Ar_2N^{2+}(^2B_1) \rightarrow N^{+}(^3P) + Ar^{+}(^2P) + Ar(^1S)$	−49.5	−53.1	9b
$He_2O^{2+}(^1A_1) \rightarrow O^{2+}(^1D) + 2He(^1S)$	+160.0[a]	+154.9[a]	10a
$He_2O^{2+}(^1A_1) \rightarrow O^{+}(^2D) + He^{+}(^2S) + He(^1S)$	−66.3[b]	−71.4[b]	10b
$Ne_2O^{2+}(^1A_1) \rightarrow O^{2+}(^1D) + 2Ne(^1S)$	+211.5[a]	+208.9[a]	11a
$Ne_2O^{2+}(^1A_1) \rightarrow O^{+}(^2D) + Ne^{+}(^2P) + Ne(^1S)$	−87.6[b]	−90.2[b]	11b
$Ar_2O^{2+}(^1A_1) \rightarrow O^{2+}(^1D) + 2Ar(^1S)$	+408.8[a]	+407.0[a]	12a
$Ar_2O^{2+}(^1A_1) \rightarrow O^{+}(^2D) + Ar^{+}(^2P) + Ar(^1S)$	−25.8[b]	−27.6[b]	12b

[a] Using the calculated energy of (^3P) O^{2+} and the experimentally determined excitation energy $^3P \rightarrow {}^1D$ (57.9 kcal/mol).[32] [b] *Using* the calculated energy of (^4S) O^+ and the experimentally determined excitation energy $^4S \rightarrow {}^2D$ (76.6 kcal/mol).[32]

= He), 56.7 kcal/mol (Ng = Ne), and 31.1 kcal/mol (Ng = Ar). The reason why the singlet state rather than triplet state is lower in energy, which is opposite to what is found for CH_2,[27] can be rationalized with the high electronegativity[28] of the noble gas elements He, Ne, and Ar.[29] It is known that substitution of hydrogen by the more electronegative fluorine in CH_2 also yields a lower lying singlet state in CF_2.[30] The decrease in the singlet–triplet energy difference from He_2C^{2+} to Ar_2C^{2+} is in line with this explanation since the electronegativities χ of the noble gases have been predicted to be $\chi(He) > \chi(Ne) > \chi(Ar)$ (see Table I).[29] Very similar results as for Ng_2C^{2+} are calculated for the diatomic ions NgC^{2+} (Table II, Chart I). Here, the $^1\Sigma^+$ state is the ground state of NgC^{2+}, and the $^3\Pi$ state is higher in energy.

Chart I. Optimized Geometries of Ng_2X^{2+} Structures at MP2/6-31G(d,p)[a]

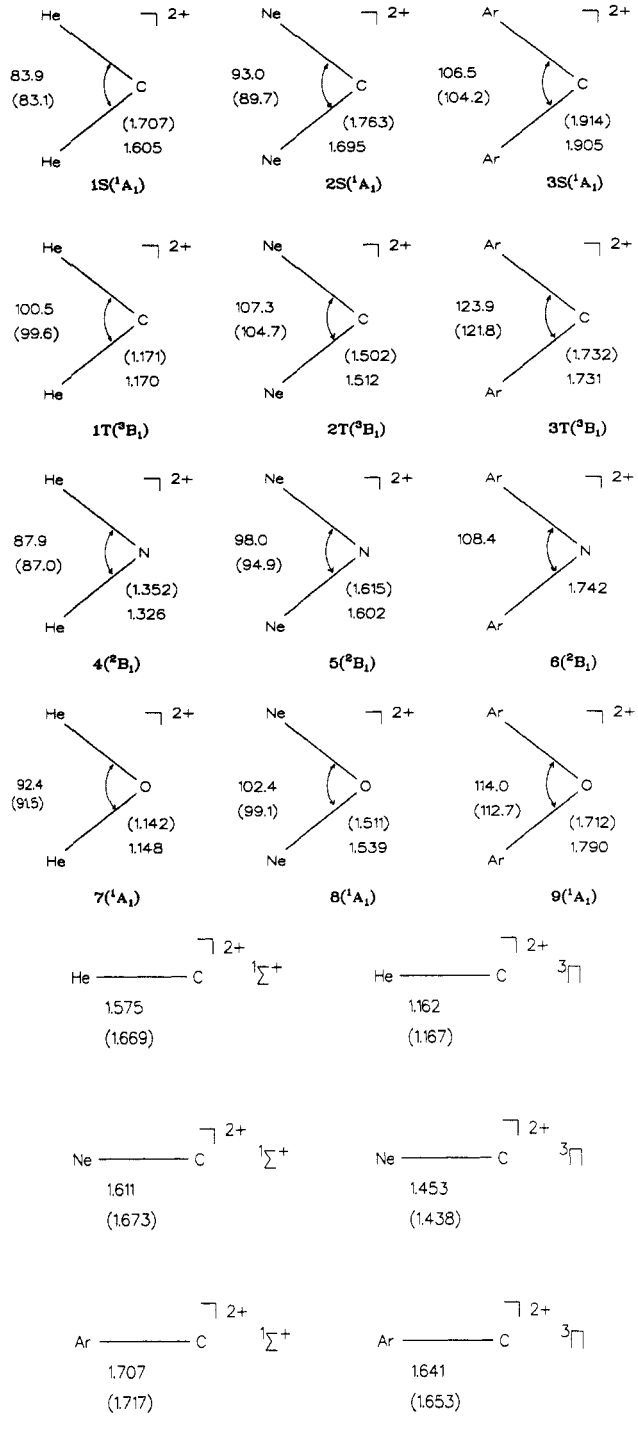

[a] HF/6-31G(d,p) values given in parentheses. Interatomic distances in Å, angles in deg.

A better insight into the interatomic interactions, which at the same time provides an explanation for the favored singlet state of Ng_2C^{2+} and NgC^{2+}, is obtained by using the model of donor–acceptor interactions.[2,3,5-7] In this model, which is based on frontier-orbital interactions,[31] the Ng_2C^{2+} structures are the result of electron donation of Ng into the empty orbitals of C^{2+}. Figure 2 shows schematically the valence orbitals of C^{2+} in the ^1S ground state and ^3P excited state. In the ^1S state, the 2s AO is doubly

(27) (a) Leopold, D. G.; Murray, K. K.; Stevens Miller, A. E.; Lineberger, W. C. *J. Chem. Phys.* **1985**, *83*, 4849. (b) Bunker, P. R.; Sears, T. J. *J. Chem. Phys.* **1985**, *83*, 4866.
(28) Frenking, G.; Koch, W. *Chem. Phys. Lett.* **1987**, *138*, 503.
(29) (a) Noyes, R. M. *J. Am. Chem. Soc.* **1963**, *85*, 2202. (b) Fung, B.-M. *J. Phys. Chem.* **1965**, *69*, 596.
(30) (a) Bauschlicher, C. W.; Schaefer, H. F.; Bagus, P. S. *J. Am. Chem. Soc.* **1977**, *99*, 7106. (b) Bauschlicher, C. W. *J. Am. Chem. Soc.* **1980**, *102*, 5492.
(31) (a) Fukui, K. *Acc. Chem. Res.* **1971**, *4*, 57. (b) Fleming, I. *Frontier Orbitals and Organic Chemical Reactions*; Wiley: Chichester, 1976.

Table II. Calculated Total Energies (E_{tot}, hartrees), Zero-Point Vibrational Energies (ZPE, kcal/mol), and Relative Energies (E_{rel}, kcal/mol) for Ng_2X^{2+} Ions

structure		state	HF/6-31G(d,p)	MP2/6-31G(d,p)		MP4(SDTQ)/6-311G(2df,2dp)	
			E_{tot}	E_{tot}	ZPE	E_{tot}[b]	E_{rel}[d]
He_2C^{2+}	**1S**	$^1A_1$	-42.1352	-42.2433	2.0	-42.3174	0.0
He_2C^{2+}	**1T**	$^3B_1$	-42.0807	-42.1630	4.9	-42.2203	63.8
Ne_2C^{2+}	**2S**	$^1A_1$	-293.4213	-293.8161	1.3	-294.1590	0.0
Ne_2C^{2+}	**2T**	$^3B_1$	-293.3482	-293.7128	2.2	-294.0400	56.7
Ar_2C^{2+}	**3S**	$^1A_1$	-1090.1485	-1090.5533	1.4	-1090.6903[a]	0.0
Ar_2C^{2+}	**3T**	$^3B_1$	-1090.1526	-1090.5218	2.2	-1090.6420[a]	31.1
He_2N^{2+}	**4**	$^2B_1$	-58.5919	-58.7246	3.6	-58.8224	
Ne_2N^{2+}	**5**	$^2B_1$	-309.8837	-310.3107	2.3	-310.6767	
Ar_2N^{2+}	**6**	$^2B_1$	[c]	1107.1257	3.6	-1107.2612[a]	
He_2O^{2+}	**7**	$^1A_1$	-78.8213	-79.0050	5.1	-79.1425	
Ne_2O^{2+}	**8**	$^1A_1$	-330.1007	-330.5930	2.6	-331.0036	
Ar_2O^{2+}	**9**	$^1A_1$	-1127.0206	-1127.5239	1.8	-1127.6691[a]	
HeC^{2+}		$^1\Sigma^+$	-39.2684	-39.3455	0.9	-39.3967	0.0
HeC^{2+}		$^3\Pi$	-39.1668	-39.2111	2.0	-39.2432	97.4
NeC^{2+}		$^1\Sigma^+$	-164.9176	-165.1427	0.9	-165.3286	0.0
NeC^{2+}		$^3\Pi$	-164.8101	-164.9989	1.2	-165.1679	101.1
ArC^{2+}		$^1\Sigma^+$	-563.3266	-563.5596	1.0	-563.6445[a]	0.0
ArC^{2+}		$^3\Pi$	-563.2721	-563.4642	1.1	-563.5324[a]	70.4
He		^1S	-2.8552	-2.8806		-2.8972	
Ne		^1S	-128.4744	-128.6262		-128.7867	
Ar		^1S	-526.7737	-526.9200		-526.9673[a]	
He^+		^2S	-1.9936	1.9936		1.9981	
Ne^+		^2P	-127.7517	-127.9494		-128.0037	
Ar^+		^2P	-526.2350	-526.3560		-526.4075[a]	
C^{2+}		^1S	-36.3992	-36.4437		-36.4710	0.0
						(-36.4708)[a]	(0.0)[a]
C^{2+}		^3P	-36.2267	-36.2323		-36.2386	145.7
						(-36.2377)[a]	(146.2)[a]
N^{2+}		^2P	-52.7956	-52.8447		-52.8906	
						(-52.8859)[a]	
O^{2+}		^3P	-73.0687	-73.1188		-73.1853	
						(-73.1749)[a]	
C^+		^2P	-37.2871	-37.3343		-37.3624	
						(-37.3580)[a]	
N^+		^3P	-53.8722	-53.9293		-53.9755	
						(-53.9653)[a]	
O^+		^4S	-74.3426	-74.4062		-74.4751	
						(-74.4576)[a]	

[a] At MP4(SDTQ)/6-311G(d,p). [b] Using MP2/6-31G(d,p) optimized geometries. [c] Not converged. [d] Including ZPE.

occupied, and only the 2p AO may accept electronic charge from Ng.

The Laplace concentration of C^{2+} (^1S) is shown in Figure 3a in the form of a perspective drawing. It shows that the C nucleus is isotropically shielded by negative charge. However, excitation of a 2s electron to a 2p orbital as in the ^3P state of C^{2+} leads to a highly anisotropic charge concentration (Figure 3b). There are two large concentration lumps in the regions where one can expect the 2p electron. Between the concentration lumps, there are deep holes in the valence shell concentration of C^{2+} (^3P), which impact to the C dication distinct electron acceptor ability. The carbon dication can pull electrons of a potential donor such as an Ng atom into its valence shell holes thus establishing an electron pair bond with Ng. In MO language, one can say that C^{2+} (^3P) possesses a low-lying singly occupied s-orbital prone to accept an electron from an Ng donor. This description establishes the basis of the donor–acceptor model used in previous work[2] to rationalize the stability of He-containing compounds. From Figure 3b it becomes immediately obvious why the Ng,C interatomic distances are significantly shorter in the $^3B_1$ ($^3\Pi$) state than in the $^1A_1$ ($^1\Sigma^+$) state of Ng_2C^{2+} (NgC^{2+}) (see Chart I).

The differences between the He, Ne, and Ar analogues of Ng_2C^{2+} and NgC^{2+} can be rationalized in the same way. The donor ability of Ng increases with He < Ne < Ar, because the energy level of the highest occupied orbital increases as evident by the ionization potential of Ng (Table I). A further difference between He and the two other elements arises from the fact that the highest occupied orbitals of Ne and Ar are p AOs and that the two latter elements may serve as p(σ) and p(π) donor. Because of the better overlap of the p(σ) AO of Ne and Ar with the empty orbitals of C^{2+}, the donor–acceptor interactions can be expected to be further enhanced. Thus, stronger interactions between Ng and C^{2+} are expected with the order He < Ne < Ar. The calculated reaction energies shown in Scheme I agree with the prediction. The ΔE_e values for dissociation of Ng_2C^{2+} ($^1A_1$) into C^{2+}(^1S) and 2Ng(^1S) are 32.6 kcal/mol (Ng = He), 71.9 kcal/mol (Ng = Ne), and 178.6 kcal/mol (Ng = Ar). For the atomization of the ($^3B_1$) triplet species Ng_2C^{2+} into C^{2+}(^3P) and 2Ng (^1S), the ΔE_e values are 117.4 kcal/mol (Ng = He), 143.0 kcal/mol (Ng = Ne), and 294.5 kcal/mol (Ng = Ar). Significant differences are also found for the dissociation energies of the $^1\Sigma^+$ and $^3\Pi$ states of NgC^{2+} (Scheme I). Thus, increasing interactions between Ng and C^{2+} are calculated for the singlet and triplet states of Ng_2C^{2+} and NgC^{2+} with the order He < Ne < Ar.

It should be pointed out that the calculated atomization energies suggest much larger differences between the properties of Ne and Ar compounds on the one hand than between those of He and Ne compounds on the other hand. Actually, this is in line with the data given in Table I, which all indicate that, chemically seen, Ne is closer to He than to Ar. Ne is a weaker electron donor and less polarizable than a fictitious element that would take the middle position between He and Ar. In addition, Ne,C bond lengths are longer than one would predict from the size of the Ne atom as reflected by the valence shell radii r_1 given in Table I. For example, the radius r_1 of He or Ar (0.34 and 0.94 Å, Table I) added to an assumed covalent radius of C of 0.7 Å leads to He,C and Ar,C bond lengths of about 1.1 and 1.6 Å, respectively. Stronger bonds should be shorter, weaker bonds longer, in line with the gross of the calculated geometries presented in this work. However, in the case of Ne,C bonds, which according to an r_1 value of 0.46

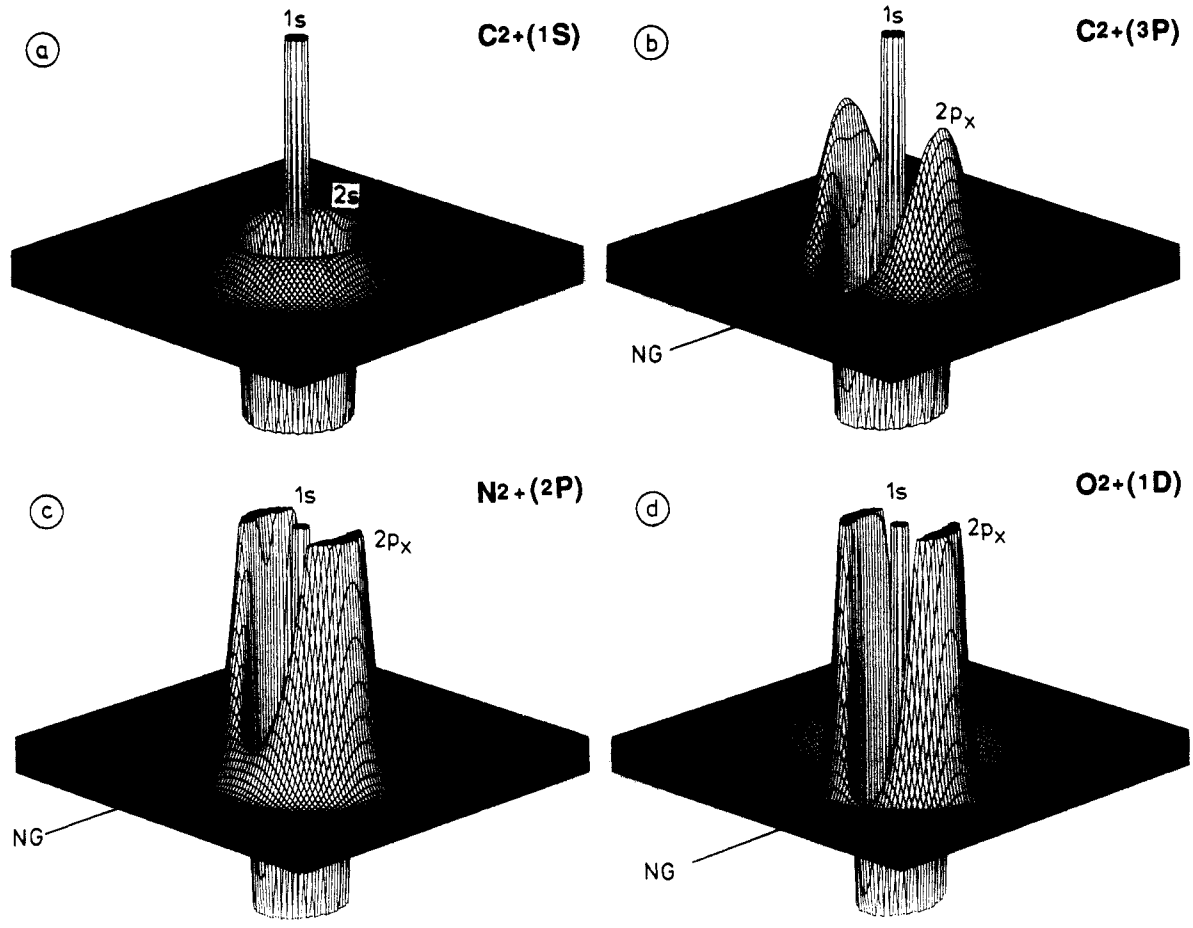

Figure 3. Perspective drawings of the HF/6-31G(d) Laplace concentration, $-\nabla^2\rho(r)$, of (a) $C^{2+}(^1S)$, (b) $C^{2+}(^3P)$, (c) $N^{2+}(^2P)$, and (d) $O^{2+}(^1D)$ influenced by an approaching Ng atom. Note that ion states change in this situation to $^1\Sigma^+$, $^3\Pi$, $^2\Pi$, and $^1\Delta$, respectively. Inner shell valence shell concentrations are indicated. Note that the function value is cut off above and below predetermined values to improve the representation.

Å (Table I) should be about 1.2 Å long, all calculated Ne,C bonds are longer by at least 0.2 Å (see **2S** and **2T** in Chart I), some of them by 0.5 Å and more (see following discussion). We interpret this bond lengthening as a result of electron repulsion involving the $2p\pi$ electrons of Ne.

Although the noble gas atoms are much stronger bound in the $^3B_1$ ($^3\Pi$) state than in the $^1A_1$ ($^1\Sigma^+$) state of Ng_2C^{2+} (NgC^{2+}), the latter is the ground state because the increase in donor–acceptor interactions for the triplet states is not sufficient to compensate for the excitation energy of C^{2+} from the ^1S to the ^3P state. The experimentally derived $^1S \rightarrow {}^3P$ excitation energy is 149.5 kcal/mol.[32] The calculated value is 145.7 kcal/mol (Table II). The largest difference of the ΔE_e values between the singlet and the triplet state of Ng_2C^{2+} for the reaction $Ng_2C^{2+} \rightarrow 2Ng + C^{2+}$, indicating the strongest increase in donor–acceptor interactions, is found for Ng = Ar (125.9 kcal/mol). Consequently, Ar_2C^{2+} has the smallest singlet–triplet gap (31.1 kcal/mol) of the three Ng_2C^{2+} species. Additional stabilization of the singlet state of Ng_2C^{2+} relative to the triplet state arises from the longer Ng,C interatomic distances, which yield lower Coulomb repulsion between the positively charged atoms. This may be the reason that Ne_2C^{2+} has a slightly smaller singlet–triplet energy gap (56.7 kcal/mol) than He_2C^{2+} (63.8 kcal/mol), although the latter exhibits a larger increase in the ΔE_e values (84.8 kcal/mol for He_2C^{2+}, reactions 1a and 2a, versus 71.1 kcal/mol for Ne_2C^{2+}, reactions 3a and 4a).

With the exception of the $^1A_1$ states of He_2C^{2+} and Ne_2C^{2+}, fragmentation of singlet and triplet Ng_2C^{2+} into the energetically lowest lying atomic products is exothermic and yields $C^+(^2P) + Ng^+ + Ng$ (Scheme I). Dissociation of **1S** is endothermic for both He and He^+ formation, where the dissociation reaction leading to He is about 5 kcal/mol less endothermic. This is because the first ionization energy of He is slightly higher than the second ionization energy of carbon (24.383 eV),[9] while Ne and Ar have lower ionization energies (Table I). The charge repulsion of the dications **1T**, **2S**, **2T**, **3S**, and **3T** is released in the energetically favored charge separation reactions 2b, 3b, 4b, 5b, and 6b (Scheme I). Dissociation of **2S** into the atomic products (reaction 3b) is thermodynamically nearly balanced, but reactions 2b, 4b, 5b, and 6b are clearly exothermic.

Analysis of the electron density distribution $\rho(r)$ reveals that all but one Ng_2C^{2+} ions investigated possess semipolar covalent Ng,C bonds (see Table III). The only exception is He_2C^{2+} in its $^1A_1$ ground state, in which He is electrostatically bound. In all other cases, necessary and sufficient condition for covalent bonding are fulfilled: Carbon atom and the two Ng atoms are connected by paths of maximum electron density, and the energy density $H(r)$ is negative at the path critical point.

There is a distinct increase of $\rho(r)$ at the path critical point of the bond Ng,C (ρ_b) when going from Ng = He to Ng = Ar. Also the value of ρ_b is significantly higher for the $^3B_1$ states than for the $^1A_1$ states. These observations are in line with calculated dissociation energies and geometries. They reflect the fact that the electron acceptor ability of C^{2+} ions is higher in the ^3P than the ^1S state and that the donor activity of Ng increases in the series He, Ne, Ar. Similar bonding features to those calculated for Ng_2C^{2+} can be found for the diatomic ions NgC^{2+}.

There is one interesting difference between He,C and Ne,C or Ar,C bonds, which becomes obvious from the calculated Laplace concentrations. In Figure 4, contour line diagrams and perspective drawings of $-\nabla^2\rho(r)$ calculated for both the $^1\Sigma^+$ and the $^3\Pi$ state of ArC^{2+} are shown. They show that in the covalently bound ions (Table III) the valence shell concentration of the Ar atom is distorted in a characteristic way. There are holes in the direction of the bond, while there are concentration lumps in the nonbonding

(32) Moore, C. E. *Atomic Energy Levels*; National Bureau of Standards, NSRDS-NBS 35; 1971.

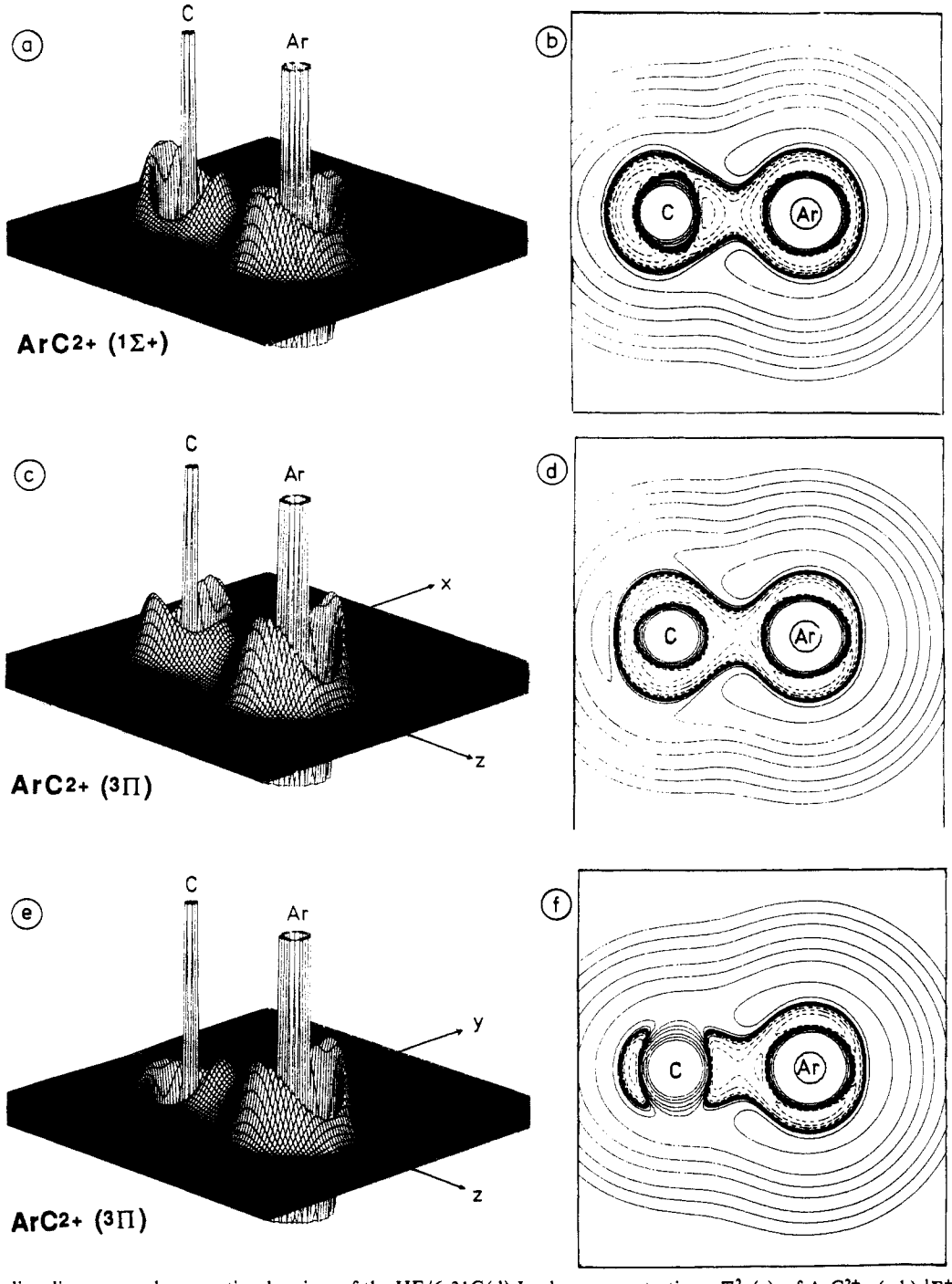

Figure 4. Contour line diagrams and perspective drawings of the HF/6-31G(d) Laplace concentration, $-\nabla^2\rho(r)$, of ArC^{2+}: (a,b) $^1\Sigma^+$ state, (c,d) $^3\Pi$ state, direction of filled π-orbital, and (e,f) $^3\Pi$ state, direction of unfilled π-orbital. In the contour line diagrams inner shell concentrations are no longer shown. In the perspective drawings, the function value is cut off above and below predetermined values to improve the representation.

region of Ar. Distortions in the valence shell concentration of the C atom are just complementary to those at the Ar atom; i.e., the concentration lumps are in the direction of the molecular axis, while the holes are in the nonbonding region. These distortions are the result of a transfer of $3p(\sigma)$ electrons from the donor Ar to the acceptor C^{2+} either into a carbon 2p (C^{2+},^{1}S) or a 2s (C^{2+},^{3}P) orbital. In the latter case, the charge transfer is more pronounced, and the concentration holes at Ar are much deeper (Figure 4d) than in the former case (Figure 4b). Figure 4 also shows that ArC^{2+} ($^3\Pi$) suffers from $2p(\pi)$–$3p(\pi)$ repulsion (see concentration lumps in the nonbonding regions of C and Ar in Figure 4f) which is absent in ArC^{2+} ($^1\Sigma^+$) (Figure 4b). Because of $p(\pi)$–$p(\pi)$ electron repulsion the Ng,C bond strength in the triplet state is almost four times as large than that in the singlet state if Ng = He, but only twice as large for Ng = Ne and less than twice as large for Ng = Ar (Table III). In the latter case it is also of importance that donation from a $3p(\sigma)$ orbital to a 2s ($2p\sigma$) orbital is less efficient than from a $2p(\sigma)$ to a 2s ($2p\sigma$) orbital.

The reason why the stabilization energies of Ng_2C^{2+} should be discussed in terms of interactions between Ng and C^{2+}, even when the most favorable dissociation products are Ng^+ and C^+, has been given before[5,6,33] and can be summarized in the following way. The potential energy curve between two singly charged ions A^+ and B^+ is essentially repulsive and exhibits an approximate $1/r$ dependency. In contrast, interactions between A^{2+} + B (and A + B^{2+}) will be attractive, and at some shorter distance r_{AB} the potential curve may become lower in energy than the $1/r$ curve

(33) Frenking, G.; Koch, W.; Liebmann, J. F. In *From Atoms to Polymers; Isoelectronic Reasoning*; Liebmann, J. F., Greenberg, A., Eds.; VCH Publishers: New York, 1989; p 169.

Table III. Characterization of NgX Bonds in Noble Gas Molecular Ions with the Aid of the Local Properties of Electron and Energy Density (HF/6-31G(d,p) Calculations)

	molecule	state	bond	r (Å)	ρ_b (e/Å^3)	H_b (hartree/Å^3)	ΔE_e[a] (kcal/mol)	bond character[c]
1S	He_2C^{2+}	$^1A_1$	HeC	1.605	0.49	−0.1	16.3	elec
1T	He_2C^{2+}	$^3B_1$	HeC	1.170	1.16	−1.2	58.7	c, semi
2S	Ne_2C^{2+}	$^1A_1$	NeC	1.695	0.71	−0.3	35.7	c, semi
2T	Ne_2C^{2+}	$^3B_1$	NeC	1.512	0.89	−1.0	71.5	c, semi
3S	Ar_2C^{2+}	$^1A_1$	ArC	1.905	0.90	−0.4	89.3	c, semi
3T	Ar_2C^{2+}	$^3B_1$	ArC	1.731	1.28	−1.1	147.3	c, semi
4	He_2N^{2+}	$^2B_1$	HeN	1.326	1.13	−0.7	43.1	c, semi
5	Ne_2N^{2+}	$^2B_1$	NeN	1.602	0.96	−0.4	66.7	c, semi
6	Ar_2N^{2+}	$^2B_1$	ArN	1.742	1.36	−0.9	138.2	c, semi
7	He_2O^{2+}	$^1A_1$	HeO	1.148	1.97	−1.9	80.0	c, semi
8	Ne_2O^{2+}	$^1A_1$	NeO	1.539	1.17	−0.4	105.7	c, semi
9	Ar_2O^{2+}	$^1A_1$	ArO	1.790	1.17	−0.5	204.4	c, semi
10a	$HeCCHe^{2+}$	$^1\Sigma_g^+$	HeC	1.085	1.38	−1.3	87.3	c, semi
10b	$HeCCHe^{2+}$	^1A_g	HeC	1.118	1.25	−1.2	89.2	c, semi
11a	$NeCCNe^{2+}$	$^1\Sigma_g^+$	NeC	1.416	0.97	−1.0	84.8	c, semi
11b	$NeCCNe^{2+}$	^1A_g	NeC	1.523	0.80	−0.9	94.9	c, semi
12a	$ArCCAr^{2+}$	$^1\Sigma_g^+$	ArC	1.648	1.53	−2.0	168.3	c, semi
12b	$ArCCAr^{2+}$	^1A_g	ArC	1.649	1.53	−2.0	168.4	c, semi
13	$HeCCH^+$	^1A	HeC	1.099	1.17	−0.9	15.4[b]	c, semi
14	$NeCCH^+$	^1A	NeC	1.507	*d*	*d*	7.1[b]	elec
15	$ArCCH^+$	^1A	ArC	1.659	1.36	−1.9	55.7[b]	c, semi
16b	$HeCN^+$	$^1\Sigma^+$	HeC	2.515	0.04	0.0	0.9[b]	elec
17b	$HeNC^+$	$^1\Sigma^+$	HeN	2.291	0.08	0.0	0.9[b]	elec
18	$NeCN^+$	$^1\Sigma^+$	NeC	2.087	0.21	−0.0	3.6[b]	elec
19	$NeNC^+$	$^1\Sigma^+$	NeN	2.113	0.24	0.0	3.6[b]	elec
20	$ArCN^+$	$^1\Sigma^+$	ArC	1.679	1.38	−1.7	35.7[b]	c, semi
21	$ArNC^+$	$^1\Sigma^+$	ArN	2.386	0.27	0.0	17.5[b]	elec

[a] Bond energies for **1–12** taken as half of the ΔE_e values of the appropriate fragmentation reactions from Schemes I and II. In the case of the $NgCCNg^{2+}$ systems, the $^1\Sigma^+(4\pi)$ state of CC^{2+} has been taken as a reference irrespective of the geometry of the noble gas compound. [b] Dissociation energies D_e taken from Schemes III and IV. [c] c and semi denote covalent, semipolar bonds; elec indicates a closed-shell interaction, e.g., electrostatic attraction due to ion-induced dipole interactions. [d] No critical point was found. Characterization of the bond on the basis of ΔE_e and $\nabla^2\rho$.

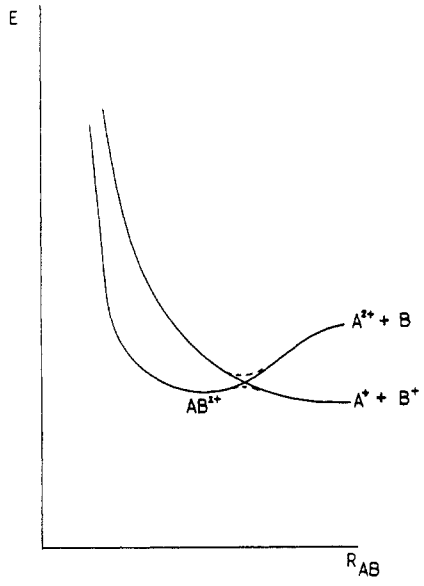

Figure 5. Schematic representation of the potential energy curves of $A^{2+} + B$ and $A^+ + B^+$.

of $A^+ + B^+$. If mixing of the two states is symmetry allowed, there will be an avoided crossing of the two curves, with the miminum energy structure largely determined by $A^{2+} + B$ ($A + B^{2+}$) interactions. This is qualitatively shown in Figure 5. In case of HeC^{2+} ($^1\Sigma^+$) the dissociation limit $He + C^{2+}$ is even lower in energy than the charge-separation products. In any case it is justified to discuss the electronic structure of AB^{2+} at the minimum energy distance in terms of interactions between $A + B^{2+}$ (or $A^{2+} + B$, depending on the ionization energies of A and B).[5,6,33]

The results for the nitrogen and oxygen analogues of Ng_2C^{2+} **4–9** are also easily understood with the help of the donor–acceptor model. In Figure 3 (parts c and d), perspective drawings of the HF/6-31G(d) Laplace concentration of N^{2+} (^2P) and O^{2+} (^1D) are shown. Both dications possess concentration holes in their valence shell, which can be filled with electrons of a suitable donor. The holes correspond to low-lying unoccupied 2p orbitals, which split into $2p(\sigma)$ and $2p(\pi)$ components upon approach of an Ng atom (Figure 3). The size of the $2p(\sigma)$ holes can be estimated by the difference $\nabla^2\rho(r)_{max} - \nabla^2\rho(r)_{min}$ where the subscripts max and min denote maximum and minimum concentration value in the valence shell. According to this difference the size increases with the atomic number, i.e., going from C^{2+} (^1S) to O^{2+} (^1D) leads to a stronger electron acceptor, which binds Ng atoms better. In MO language, one can say that the $2p(\sigma)$ MO becomes lower in energy, and, hence, frontier orbital interactions between donor and acceptor increase.

This is exactly what is calculated for the dissociation of the ground states of Ng_2X^{2+} into $2Ng + X^{2+}$. All ions with X = N and X = O possess covalent bonds according to the data given in Table III. The ΔE_e values shown in Scheme I for He_2X^{2+} are 32.6 kcal/mol (X = C; $^1A_1$), 86.2 kcal/mol (X = N), and 160.0 kcal/mol (X = O); for Ne_2X^{2+} ΔE_e is 71.9 kcal/mol (X = C; $^2B_1$), 133.4 kcal/mol (X = N), and 211.5 kcal/mol (X = O); for Ar_2X^{2+} the ΔE_e values are 178.6 kcal/mol (X = C; $^1A_1$), 276.4 kcal/mol (X = N), and 408.8 kcal/mol (X = O). For each atom X investigated, the difference in ΔE_e values is much greater between Ne_2X^{2+} and Ar_2X^{2+} than between He_2X^{2+} and Ne_2X^{2+}. This is also reflected by the bond energies shown in Table III, which have been derived from ΔE_e values from Scheme I.

The increase in Ng,X donor–acceptor interactions in the ground states of Ng_2X^{2+} with C < N < O is also reflected by the changes in the calculated geometries (Chart I). The Ng,X distance decreases, and the Ng,X,Ng angle increases from Ng = He to Ng = Ar. In summary, the changes in the electronic structure, stability, and geometry of the Ng_2X^{2+} ions **1S–9** can be rationalized by invoking interactions between Ng and X^{2+} in the corresponding electronic state.

3.2. Doubly Charged Acetylene Analogues $NgCCNg^{2+}$. The dramatic increase in Ng,C bond energies when going from the ^1S ground state to the ^3P excited state of C^{2+} (see Table III) indicates the importance of low-lying empty σ orbitals (σ holes

Scheme II. Calculated Fragmentation Energies (ΔE_e and ΔE_o, kcal/mol) at MP4(SDTQ)/6-311(2df,2pd)//MP2/6-31G(d,p) (Helium and Neon Structures) MP4(SDTQ)/6-311G(d,p)//MP2/6-31G(d,p) (Argon Structures) for $NgCCNg^{2+}$ Molecules

reaction	ΔE_e	ΔE_o	no.
$HeCCHe^{2+}$ (**10a**) → 2He (^1S) + CC^{2+} ($^1\Sigma^+_g$, 4π)	+174.6		13a
$HeCCHe^{2+}$ (**10a**) → 2He (^1S) + CC^{2+} ($^1\Sigma^+_g$, oπ)	+18.9	+10.0	13b
$HeCCHe^{2+}$ (**10a**) → He (^1S) + He^+ (^2S) + CC^+($^2\Pi_u$)	+86.0	+78.6	13c
$HeCCHe^{2+}$ (**10a**) → $2HeC^+$ ($^2\Pi$)	−103.6	−112.6	13d
$HeCCHe^{2+}$ (**10b**) → 2He (^1S) + CC^{2+} ($^1\Sigma^+_g$, 4Π)	+178.5		14a
$HeCCHe^{2+}$ (**10b**) → 2He (^1S) + CC^{2+} ($^1\Delta_g$)	+58.2[a]		14b
$HeCCHe^{2+}$ (**10b**) → 2He (^1S) + CC^{2+} ($^1\Sigma^+$, oπ)	+22.8	+14.2	14c
$HeCCHe^{2+}$ (**10b**) → He (^1S) + He^+ (^2S) + CC^+ ($^2\Pi_u$)	+89.9	+82.8	14d
$HeCCHe^{2+}$ (**10b**) → $2HeC^+$ ($^2\Pi$)	−99.7	−108.6	14e
$NeCCNe^{2+}$ (**11a**) → 2Ne (^1S) + CC^{2+} ($^1\Sigma^+_g$, 4π)	+169.6		15a
$NeCCNe^{2+}$ (**11a**) → 2Ne (^1S) + CC^{2+} ($^1\Sigma^+_g$, oπ)	+13.9	+8.3	15b
$NeCCNe^{2+}$ (**11a**) → Ne (^1S) + Ne^+ (^2P) + CC^+ ($^2\Pi_u$)	+8.2	+4.1	15c
$NeCCNe^{2+}$ (**11a**) → $2NeC^+$ ($^2\Pi$)	−116.0	−121.5	15d
$NeCCNe^{2+}$ (**11b**) → 2Ne (^1S) + CC^{2+} ($^1\Sigma^+_g$, 4Π)	+189.9		16a
$NeCCNe^{2+}$ (**11b**) → 2Ne (^1S) + CC^{2+} ($^1\Delta_g$)	+75.6[a]		16b
$NeCCNe^{2+}$ (**11b**) → 2Ne (^1S) + CC^{2+} ($^1\Sigma^+_g$, oπ)	+34.2	+28.4	16c
$NeCCNe^{2+}$ (**11b**) → Ne (^1S) + Ne^+ (^2P) + CC^+ ($^2\Pi_u$)	+28.5	+24.2	16d
$NeCCNe^{2+}$ (**11b**) → $2NeC^+$ ($^2\Pi$)	−95.6	−101.6	16e
$ArCCAr^{2+}$ (**12a**) → 2Ar (^1S) + CC^{2+} ($^1\Sigma^+_g$, 4π)	+336.7		17a
$ArCCAr^{2+}$ (**12a**) → 2Ar (^1S) + CC^{2+} ($^1\Sigma^+_g$, oπ)	+173.4	+168.2[b]	17b
$ArCCAr^{2+}$ (**12a**) → Ar (^1S) + Ar^+ (^2P) + CC^+ ($^2\Pi_u$)	+34.9	+31.2[b]	17c
$ArCCAr^{2+}$ (**12a**) → $2ArC^+$ ($^2\Pi$)	+14.3	+9.4[b]	17d
$ArCCAr^{2+}$ (**12b**) → 2Ar (^1S) + CC^{2+} ($^1\Sigma^+_g$, 4Π)	+336.6		18a
$ArCCAr^{2+}$ (**12b**) → 2Ar (^1S) + CC^{2+} ($^1\Delta_g$)	+222.8[a]		18b
$ArCCAr^{2+}$ (**12b**) → 2Ar (^1S) + CC^{2+} ($^1\Sigma^+_g$, oπ)	+173.3	+168.1	18c
$ArCCAr^{2+}$ (**12b**) → Ar (^1S) + Ar^+ (^2P) + CC^+ ($^2\Pi_u$)	+34.8	+31.1	18d
$ArCCAr^{2+}$ (**12b**) → $2ArC^+$ ($^2\Pi$)	+14.2	+9.3	18e

[a] At MP2/6-31G(d,p), using complex orbitals for $CC^{2+}(^1\Delta_g)$. [b] Using ZPE data of structure **6b**.

Chart II. Optimized Geometries of $NgCCNg^{2+}$ Structures and Dissociation Products at MP2/6-31G(d,p) (HF/6-31G(d,p))[a]

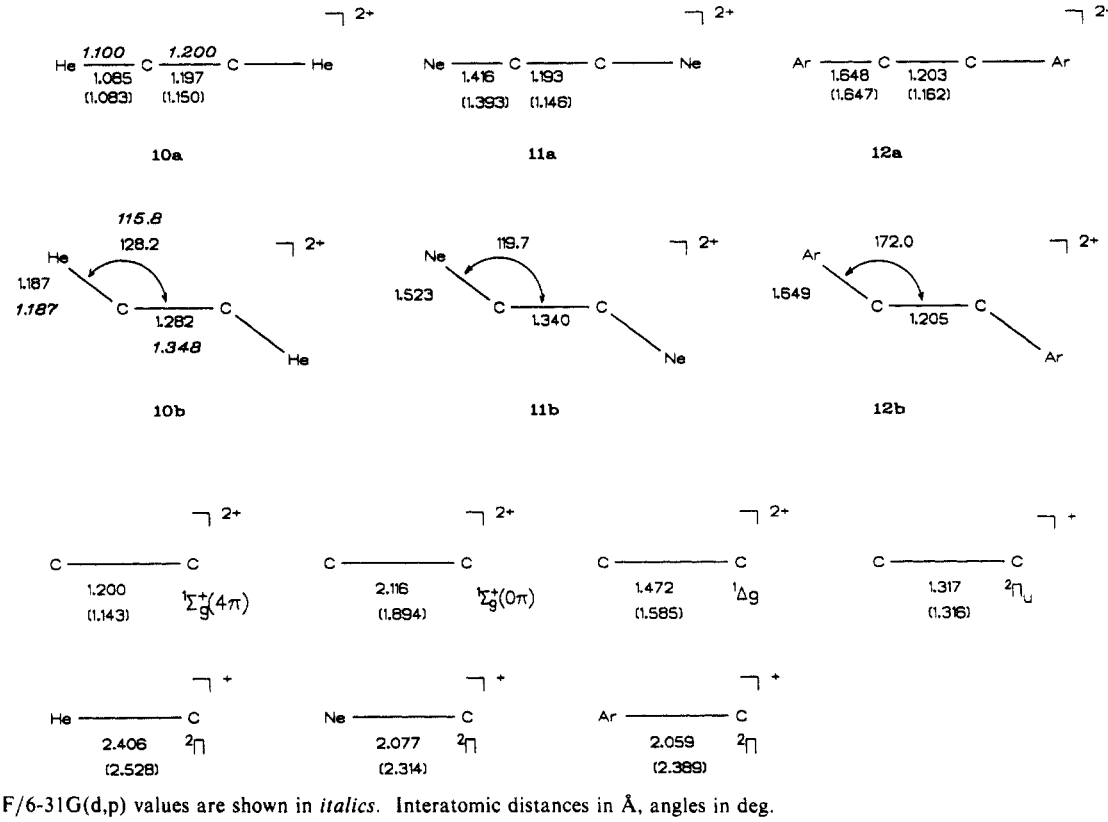

[a] CASSCF/6-31G(d,p) values are shown in *italics*. Interatomic distances in Å, angles in deg.

in the valence sphere) to be used by the acceptor to pull electrons from Ng in its valence shell, thereby binding the Ng atom. In case of Ng_2C^{2+}, the increase is not sufficient to compensate for the excitation energy of C^{2+} ($^1S \rightarrow {}^3P$), and the weaker bound $^1A_1$ state of Ng_2C^{2+} is lower in energy than the stronger bound $^3B_1$ state. In our previous investigation of helium compounds[2] we found that CC^{2+} is an even better acceptor than C^{2+}. For example, $HeCCHe^{2+}$ ($^1\Sigma^+_g$), **10a**, which is isoelectronic with acetylene, has a calculated He,C distance of only 1.085 Å and is *lower* in energy than the ground state of CC^{2+} ($^1\Sigma^+_g,0\pi$) + 2He.[2] Figure 6 shows schematically the orbital diagrams of CC^{2+} in several electronic states.

The electronic structure of $HeCCHe^{2+}$ (**10a**) corresponds to that of the excited $^1\Sigma^+_g(4\pi)$ state of CC^{2+} (Figure 6). This state has a very low-lying empty $2\sigma_u$ orbital which interacts strongly with the 1s AO of He. The fragmentation energy ΔE_o of **10a** into CC^{2+} ($^1\Sigma^+_g(4\pi)$) + 2He is 174.6 kcal/mol (reaction 13a, Scheme II). This corresponds to a He,C bond energy of 87.3 kcal/mol

Table IV. Calculated Total Energies (E_{tot}, hartrees), Zero-Point Vibrational Energies (ZPE, kcal/mol), and Relative Energies (E_{rel}, kcal/mol) for $NgCCNg^{2+}$ Cations

structure		state	HF/6-31G(d,p)	MP2/6-31G(d,p)		MP4/6-311G(2df,2pd)		CASSCF/6-31G(d,p)	
			E_{tot}	E_{tot}	ZPE	E_{tot}[e]	E_{rel}[f]	E_{tot}	E_{rel}
$HeCCHe^{2+}$	**10a**	$^1\Sigma_g^+$	−79.9786	−80.2549	9.4	−80.3578	0.0	−80.1646	0.0
$HeCCHe^{2+}$	**10b**	^1A		−80.2561	9.1	−80.3640	−4.2	−80.1807	−10.1
$NeCCNe^{2+}$	**11a**	$^1\Sigma_g^+$	−331.2076	−331.7612	6.1	−332.1288	0.0		
$NeCCNe^{2+}$	**11b**	^1A_g		−331.7751	6.3	−332.1613	−20.2		
$ArCCAr^{2+}$	**12a**	$^1\Sigma_g^+$	−1128.0424	−1128.5973[b]		−1128.7300[d]	0.0		
$ArCCAr^{2+}$	**12b**	^1A_g		−1128.5974	5.7	−1128.7299[d]	0.1[g]		
CC^{2+}		$^1\Sigma_g^+(4\pi)$	−74.0169	−74.2193		−74.2850 (−74.2584)[d]			
CC^{2+}		$^1\Delta_g$	−74.1804[a]	−74.4021[a]					
CC^{2+}		$^1\Sigma_g^+(0\pi)$	−74.3007	−74.4462	0.5	−74.5333 (−74.5188)[d]			
CC^+		$^2\Pi_u(3\pi)$	−74.9770	−75.2500	2.0	−75.3253 (−75.2995)[d]			
HeC^+		$^2\Pi$	−40.1430	−40.2161	0.2	−40.2615			
NeC^+		$^2\Pi$	−165.7661	−165.9700	0.3	−166.1569			
ArC^+		$^2\Pi$	−564.0698	−564.2777	0.4	−564.3536[d]			

[a] Complex orbitals. [b] Not a minimum structure (see text). [c] Linear ($^1\Sigma^+$) minimum structure. [d] At MP4/6-311G(d,p). [e] Using MP2/6-31G(d,p) optimized geometries. [f] Including ZPE. [g] Without ZPE.

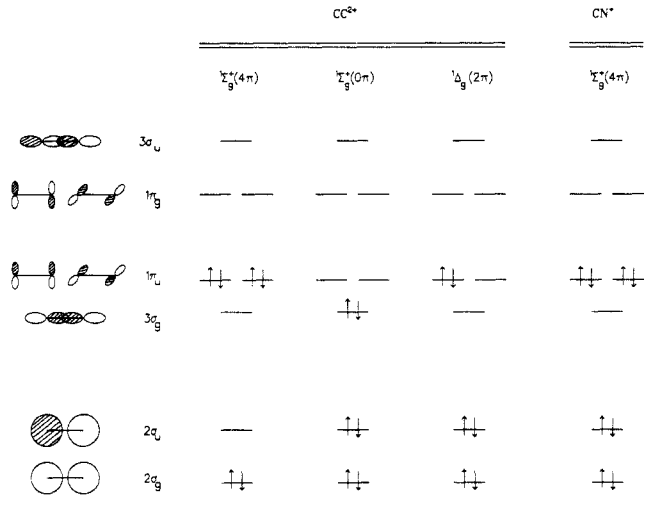

Figure 6. Schematic representation of the molecular orbitals of CC^{2+} and CN^{2+}. Only one resonance structure for the π-electrons of the $^1\Delta_g$ state of CC^{2+} is shown.

which is sufficient to compensate for the excitation energy $CC^{2+}(^1\Sigma^+_g(0\pi)) \rightarrow CC^{2+}(^1\Sigma^+_g(4\pi))$.

In contrast, the ground state of CC^{2+} ($^1\Sigma^+_g(0\pi)$) does not form a $HeCCHe^{2+}$ minimum energy structure.[34] This can be explained by the absence of a low-lying empty orbital for CC^{2+} ($^1\Sigma^+_g(0\pi)$). But what about other electronic states such as the $^1\Delta_g$ state of CC^{2+} (Figure 6)? In ref 2 it was demonstrated that π-type concentration holes are formed in the valence shell of CC^{2+} ($^1\Delta_g$) upon approach of Ng atoms (see ref 2, Figure 8). Reactions of CC^{2+} ($^1\Delta_g$) with one or two noble gas atoms should lead to nonlinear structures. In fact, a nonlinear form of $HeCC^{2+}$ was found to be a true energy minimum at MP2/6-31G(d,p), 39.1 kcal/mol lower in energy than the linear ($^1\Sigma^+$) form.[2] Therefore, we have also searched for nonlinear forms of $NgCCNg^{2+}$.

At HF/6-31G(d,p), only the linear forms **10a**, **11a**, and **12a** have been found as minima on the respective $NgCCNg^{2+}$ potential energy surface. However, trans-bent structures for $HeCCHe^{2+}$ (**10b**), $NeCCNe^{2+}$ (**11b**), and $ArCCAr^{2+}$ (**12b**) as shown in Chart II are calculated to represent energy minima on the $NgCCNg^{2+}$ potential surfaces at MP2/6-31G(d,p). In none of these cases has an energy minimum with a cis geometry been found. The trans-bent forms are lower in energy than the linear $NgCCNg^{2+}$ structures for Ng = He by 4.2 kcal/mol and for Ng = Ne by 20.2 kcal/mol (Table IV). The calculated gain in energy upon bending when going from $HeCCHe^{2+}$ to $NeCCNe^{2+}$ is due to the reduction of $2p\pi(Ne)-2p\pi(C)$ repulsion important for **11** but not for **10**.

In the case of $ArCCAr^{2+}$, the linear and the trans-bent forms **12a** and **12b** have nearly the same energy (Table IV), structure **12b** being either 0.06 kcal/mol more stable (MP2/6-31G(d,p) or 0.06 kcal/mol less stable than **12a** (MP4/6-311G(d,p)). These energies indicate that $2p\pi(C)-3p\pi(Ar)$ electron repulsion is less important than $2p\pi(C)-2p\pi(Ne)$ electron repulsion. The effect of $2p\pi(C)-2p\pi(Ne)$ electron repulsion in **11a** is also reflected by the calculated fragmentation energies of $NgCCNg^{2+}$ into CC^{2+} + 2Ng (Scheme II). For the linear forms, the dissociation energy of $NeCCNe^{2+}$ (**11a**) into $CC^{2+}(^1\Sigma^+_g,4\pi)$ + 2Ne is *lower* than for $HeCCHe^{2+}$ (**10a**) yielding $CC^{2+}(^1\Sigma^+_g,4\pi)$ + 2He (reactions 13a and 15a, Scheme II). For the bent forms **10b** and **11b**, the dissociation energy for fragmentation into $CC^{2+}(^1\Delta_g)$ + 2Ng is *higher* for Ng = Ne than for Ng = He (reactions 14a and 16a, Scheme II).

In order to ascertain that the trans-bent structure of $HeCCHe^{2+}$ is not an artifact of the MP approach, we have performed CASSCF/6-31G(d,p) calculations (Table IV and Chart II). These calculations confirm the trans-bent structure for **10**, predicting **10b** to be 10.4 kcal/mol more stable than **10a**. This value is probably somewhat too high caused by an insufficient treatment of dynamic electron correlation at the CASSCF level and the smaller basis set. At MP4/6-311G(2df,2pd), we calculate an energy difference of just 4.2 kcal/mol.

We have also calculated $HeCCHe^{2+}$ with bond angles HeCC fixed at intermediate values between **10a** and **10b**. At MP2/6-31G(d,p), the potential energy surface is very flat. The energy difference between **10a** ($\angle_{HeCC}$ = 180°) and **10b** ($\angle_{HeCC}$ = 128.2°) is only 0.8 kcal/mol. At $\angle_{HeCC}$ = 155.2°, we located a transition state structure only 1.1 kcal/mol higher in energy than **10b** and 0.3 kcal/mol less stable than **10a**. At MP4/6-311G(2df,2pd)//MP2/6-31G(d,p), the energy of the transition-state structure is even 0.1 kcal/mol *lower* than **10a**. This means that the linear form **10a**, although it is an energy minimum at MP2/6-31G(d,p), is probably not an energy minimum species at higher levels of theory. The same holds true for $NeCCNe^{2+}$. At MP2/6-31G(d,p), we located a transition-state structure for the isomerization between **11a** and **11b** at $\angle_{NeCC}$ = 166.7° which is only 0.1 kcal/mol higher in energy than **11a**. Single-point calculations at MP4(SDTQ)/6-311G(d,p) show that this "transition state" is 9.4 kcal/mol lower in energy than **11a**. These results indicate that only the trans-bent structures **10b** and **11b**, but probably not the linear forms **10a** and **11a**, are energy minimum species.

One might think that the trans-bent form **10b** is related to excited states of acetylene, which also possess a trans-bent geometry.[35-37] It is important to point out that the nonlinear geometry of the first excited state of acetylene is caused by the occupation of the CC antibonding π_g MOs one of which becomes

(34) The optimization of a linear structure $HeCCHe^{2+}$ corresponding to the $^1\Sigma^+_g$ (0π) state of CC^{2+} yields two separated HeC^+ ions.

Chart III. Optimized Geometries of $NgCCH^+$ Structures and Dissociation Products at MP2/6-31G(d,p) (HF/6-31G(d,p))[a]

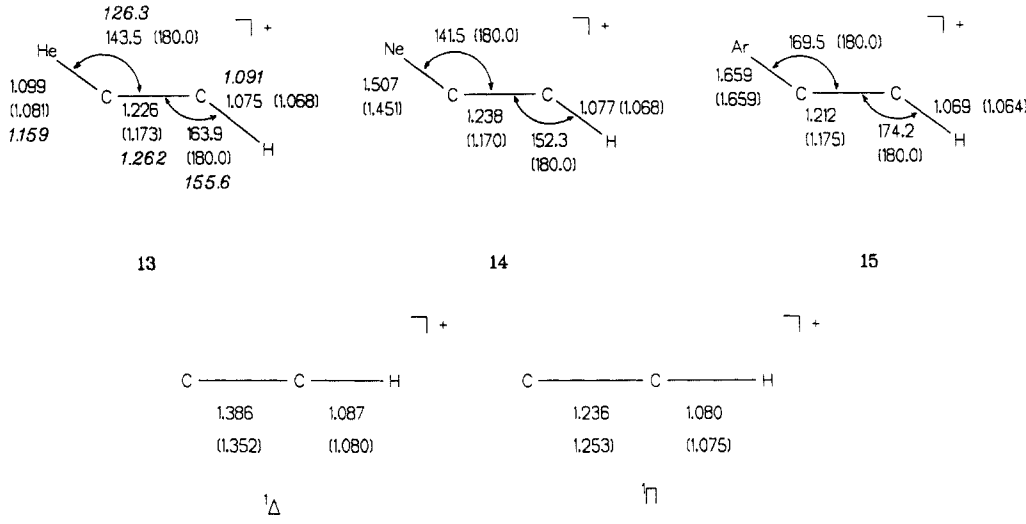

[a] CASSCF/6-31G(d,p) values are shown in *italics*. Interatomic distances in Å, angles in deg.

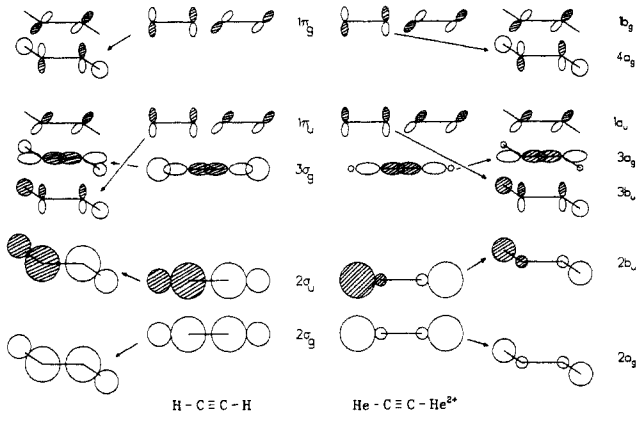

Figure 7. Orbital correlation diagrams for bending of (a) acetylene and (b) $HeCCHe^{2+}$.

CH-bonding and thus stabilizing upon bending of the molecule (see Figure 7). However, none of the π_g MOs is occupied in $NgCCNg^{2+}$ (^1A_g).

Normally, a 10 valence electron system such as acetylene HCCH possesses a linear structure, which can easily be explained on the basis of MO correlation diagrams (Figure 7a).[38] The three bonding σ MOs are predominantly CC bonding ($2\sigma_g$), CH bonding ($2\sigma_u$), and CH bonding ($3\sigma_g$).[39] The latter MO is formed by bonding overlap of $2p\sigma$(C) orbitals, which means that bending of acetylene leads to a decrease of CH bonding and, hence, to an increase of the molecular energy.

In the case of $NgCCNg^{2+}$, the three σ MOs possess NgC bonding ($2\sigma_g$), NgC bonding ($2\sigma_u$), and CC bonding ($3\sigma_g$) character (Figure 7b); i.e., bending of the molecule leads only to a moderate, if at all, increase of the energy of the $3\sigma_g$ MO since its contribution to NgC bonding is only of minor importance.[39] At the same time, the in-plane π_u MO can overlap in a bonding fashion with σ-type Ng orbitals upon bending of the molecule, thus stabilizing the nonlinear form. Since antibonding overlap between nonnearest neighbors is minimized in the trans-bent form, it is evident that this structure represents the energy minimum of the $NgCCNg^{2+}$ molecules. *The trans-bent equilibrium geometries of* ***10*** *and* ***11*** *are due to the electronegativity difference between noble gas atom and carbon and the corresponding shape of the* σ *Mos.*

All Ng,C bonds in the linear and trans-bent forms of $NgCCNg^{2+}$ are covalent. This is suggested by the properties of the electron density evaluated at the bond critical points (Table III). The density data also reflect the fact that the Ne,C bond is actually weaker than the He,C bond due to $2p(\pi)-\pi_u$ electron repulsion absent in the He compound. Analysis of the electron density distribution confirms that Ng,C bonding in $NeCCNe^{2+}$ and $ArCCAr^{2+}$ is due to $p(\sigma)$ electron donation from Ng. Figure 8a depicts a perspective drawing of the calculated Laplace concentration of $ArCCAr^{2+}$ (**12a**). There are concentration holes in the valence shell of the Ar atom where one would expect the $3p\sigma$ electrons, and there are concentration lumps in the regions of the $3p\pi$ electrons. Furthermore, there is a distinct increase of electron concentration in the Ar,C bond region indicative of a semipolar covalent bond between Ng and C. Similar features can be observed in the Laplace concentration of $NeCCNe^{2+}$ although the Ne atoms are still surrounded in the molecule by the outer depletion sphere, which is now less pronounced than in the free atom (Figure 8b).

All $NgCCNg^{2+}$ ions are thermodynamically stable toward loss of the Ng atoms. The energetically lowest lying products in case of $HeCCHe^{2+}$ (**10b**) are CC^{2+} ($^1\Sigma^+_g,0\pi$) + 2He (ΔE_o = 14.2 kcal/mol, Scheme II). For $NeCCNe^{2+}$ (**11b**), the most stable fragmentation products for loss of Ng atoms are $CC^+(^2\Pi_u)$[40] + Ne + Ne^+ (ΔE_o = 24.2 kcal/mol). Both ions are thermodynamically unstable toward dissociation into $2NgC^+(^2\Pi)$ by −108.6 kcal/mol (Ng = He) and −101.6 kcal/mol (Ng = Ne, Scheme II). However, $ArCCAr^{2+}$ is even stable when breaking the C,C bond (ΔE_o = 9.3 kcal/mol, reaction 18d, Scheme II). The higher stability of the argon analogue is another indication of the significantly stronger donor–acceptor interactions between Ar and the acceptor X as compared to those between Ne or He and X.

3.3. Singly Charged Acetylene Analogues $NgCCH^+$. In our previous theoretical study we found[2] that helium may be covalently bound not only to doubly charged binding partners but also to singly charged cations. An example is the isoelectronic acetylene analogue $HeCCH^+$ (**13**). At the Hartree–Fock level, **13** is predicted to have a linear geometry with a short He,C distance of 1.081 Å. With inclusion of correlation corrections at MP2/6-31G(d,p), $HeCCH^+$ (**13**) is calculated with a trans-bent geometry and a slightly larger He,C distance of 1.099 Å (Chart III). We have optimized **13** also at the CASSCF/6-31G(d,p) level. The results in Chart III show that the He,C distance is longer (1.159 Å), and the bond angles become smaller compared with the data obtained at MP2/6-31G(d,p). At both levels, MP2/6-31G(d,p)

(35) Lischka, H.; Karpfen, A. *Chem. Phys.* **1986**, *102*, 77.
(36) So, S. P.; Wetmore, R. W.; Schaefer, H. F., III *J. Chem. Phys.* **1980**, *73*, 5706.
(37) (a) King, G. W.; Ingold, C. K. *Nature* **1952**, *169*, 1101. (b) Ingold, C. K.; King, G. W. *J. Chem. Soc.* **1953**, 2702. (c) Innes, K. K. *J. Chem. Phys.* **1954**, *22*, 863.
(38) Gimarc, B. M. *Molecular Structure and Bonding*; Academic Press: New York, 1979.
(39) See Figure 4 of ref 2.

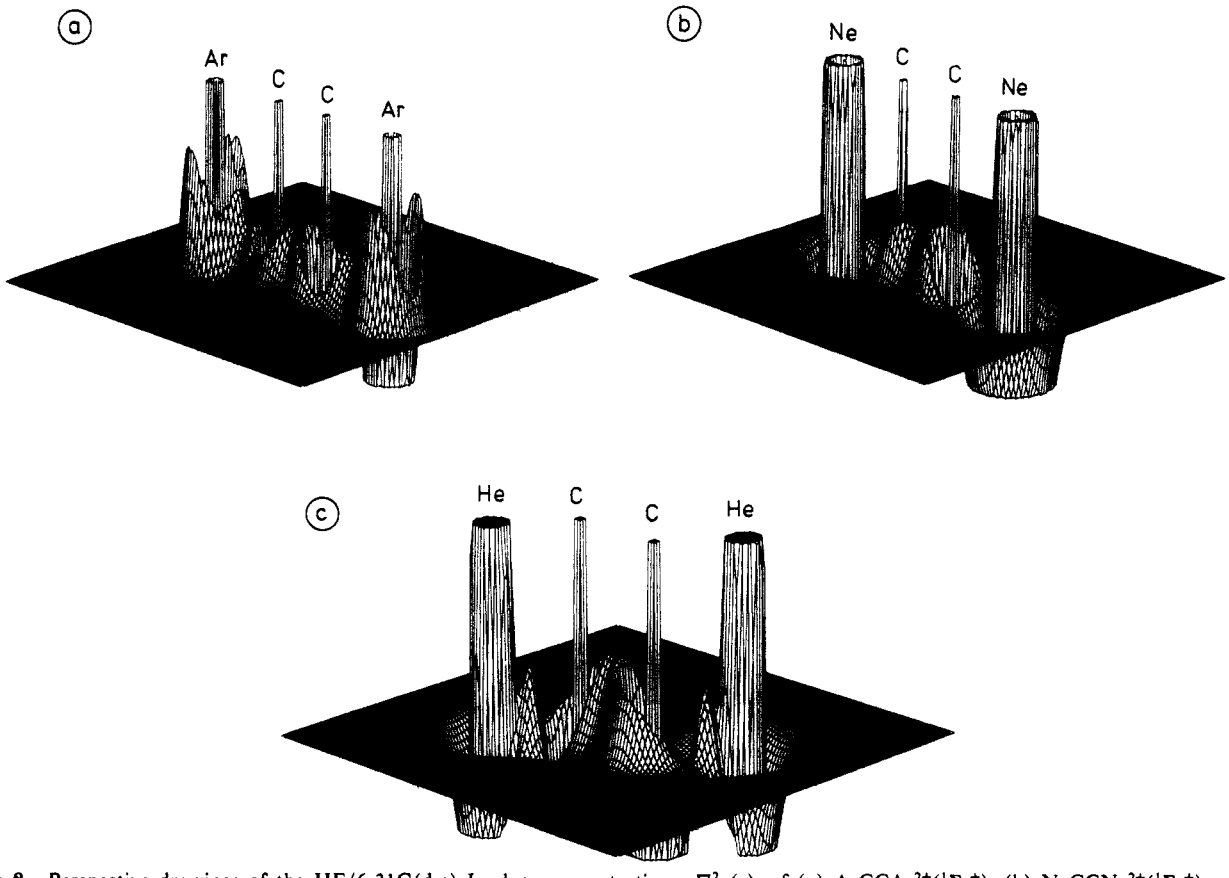

Figure 8. Perspective drawings of the HF/6-31G(d,p) Laplace concentration, $-\nabla^2\rho(r)$, of (a) $ArCCAr^{2+}(^1\Sigma_g^+)$, (b) $NeCCNe^{2+}(^1\Sigma_g^+)$, and (c) $HeCCHe^{2+}(^1A_g)$. Inner shell and valence shell concentrations are indicated. Note that the function value is cut off above and below predetermined values to improve the representation.

Table V. Calculated Total Energies (E_{tot}, hartrees) and Zero-Point Vibrational Energies (ZPE, kcal/mol) for $NgCCH^+$ Cations

structure		state	HF/6-31G(d,p) E_{tot}	MP2/6-31G(d,p) E_{tot}	MP2/6-31G(d,p) ZPE	MP4/6-311G(2df,2pd) E_{tot}[d]	CASSF/6-31G(d,p) E_{tot}
$HeCCH^+$	**13**	$^1A'$	-78.5586[c]	-78.8295	12.0	-78.9305	-78.7265
$NeCCH^+$	**14**	$^1A'$	-204.1556[c]	-204.5673	10.3	-204.8068	
$ArCCH^+$	**15**	$^1A'$	-602.5331[c]	-602.9417	10.5	-603.0304[b]	
CCH^+		$^1\Delta$	-75.7290[a]	-75.9111[a]			
CCH^+		$^1\Pi$	-75.7627	-75.9318	9.1	-76.0087 (-75.9743)[b]	-75.8474

[a] Complex orbitals. [b] At MP4/6-311G(d,p). [c] Linear ($^1\Sigma^+$) minimum structure. [d] Using MP2/6-31G(d,p) optimized geometries.

and CASSCF/6-31G(d,p), the He,C distance in **13** is slightly longer than in linear $HeCCHe^{2+}$ (**10a**) but shorter compared with trans bent **10b** (Chart II).

$NeCCH^+$ (**14**) and $ArCCH^+$ (**15**) are also calculated with a trans-bent geometry. The bond angles are smaller in **14** than in **13** but become larger in **15**. As in the analogous helium ions, the Ne,C distance in **14** is larger than in linear $NeCCNe^{2+}$ (**11a**) but shorter than in the trans bent form **11b** (Chart II). The Ar,C distance in the singly charged cation **15** is similar to the value predicted for doubly charged **12a** and **12b** (Chart II).

The trans-bent structure of $NgCCH^+$ can be rationalized in the same way as the nonlinear structure of $NgCCNg^{2+}$ discussed in the previous section. The MO correlation diagram in Figure 7 reveals also that due to the larger electronegativity of He compared to that of H the HeCC bending angle should be much smaller than the HCC angle. This is confirmed by the calculated bond angles shown in Chart III.

In the case of $NeCCH^+$ (**14**) bending of the molecule leads to an overlap of the $2p\sigma$(Ne) orbital and the in-plane π_u MO of the CC unit. Sufficient overlap can only be achieved if the bending angle is smaller than that of $HeCCH^+$. In addition to an improvement of bonding Ne,C overlap, angle bending leads also to a reduction of electron repulsion between the lone pair electrons of Ne and the π-electrons of the CC unit. Again, $p(\pi)$-$p(\pi)$ electron repulsion is stronger for the Ne compound **14** than the Ar compound **15** (see above). As a consequence, the ArCC angle is close to 180°, while the NeCC angle is smaller than the HeCC angle (see calculated geometries in Chart III).

Scheme III. Calculated Dissociation Energies (D_e and D_0; kcal/mol) at MP4(SDTQ)/6-311G(2df,2pd)//MP2/6-31G(d,p) (Helium and Neon Structures), MP4(SDTQ)/6-311G(d,p)//MP2/6-31G(d,p) (Argon Structures) for $NgCCH^+$ Molecules

reaction	D_e	D_0	no.
$HeCCH^+$ (**13**) → He (^1S) + CCH^+ ($^1\Delta$)	23.7[a]		19a
$HeCCH^+$ (**13**) → He (^1S) + CCH^+ ($^1\Pi$)	15.4 (15.0)[b]	12.5	19b
$NeCCH^+$ (**14**) → Ne (^1S) + CCH^+ ($^1\Delta$)	18.8[a]		20a
$NeCCH^+$ (**14**) → Ne (^1S) + CCH^+ ($^1\Pi$)	7.1	5.9	20b
$ArCCH^+$ (**15**) → Ar (^1S) + CCH^+ ($^1\Delta$)	69.4[a]		21a
$ArCCH^+$ (**15**) → Ar (^1S) + CCH^+ ($^1\Pi$)	55.7	54.3	21b

[a] At MP2/6-31G(d,p)//MP2/6-31G(d,p), using complex orbitals for CCH^+. [b] At CASSCF/6-31G(d,p).

The importance of $p(\pi)$-$p(\pi)$ electron repulsion in Ne compounds is reflected by the calculated Ng,C dissociation energies of $NgCCH^+$ ions (Scheme III). Dissociation of $NgCCH^+$ into Ng and $CCH^+(^1\Pi)$ is endoenergetic by 15.4, 7.1, and 55.7 kcal/mol, and dissociation into Ng and $CCH^+(^1\Delta)$ is endoenergetic by 23.7, 18.8, and 69.4 kcal/mol for Ng = He, Ne, Ar, respectively (Scheme III). Reexamination of the singlet states of CCH^+ has shown that the $^1\Pi$ state of this cation is lower in energy than the

Table VI. Calculated Total Energies (E_{tot}; hartrees) and Zero-Point Vibrational Energies (ZPE, kcal/mol) for $NgCN^+$ and $NgNC^+$ Ions

structure		state	HF/6-31G(d,p)	MP2/6-31G(d,p)		MP4(SDTQ)/6-311G(2df,2pd)	
			E_{tot}	E_{tot}	ZPE	E_{tot}[b]	E_{rel}[c]
$HeCN^+$	**16a**	$^1\Sigma^+$	−94.5319	−94.8461	4.6	−94.9534	0.0
$HeCN^+$	**16b**	$^1\Sigma^+$		−94.8610	3.4	−94.9835	−20.1
$HeNC^+$	**17a**	$^1\Sigma^+$	−94.4512				
$HeNC^+$	**17b**	$^1\Sigma^+$	−94.4676	−94.8612	3.6	−94.9835	−19.9
$NeCN^+$	**18**	$^1\Sigma^+$	−220.1400	−220.6163	4.7	−220.8773	0.0
$NeNC^+$	**19**	$^1\Sigma^+$	−220.0883	−220.6147	4.5	−220.8772	−0.1
$ArCN^+$	**20**	$^1\Sigma^+$	−618.5324	−618.9803	4.5	−619.0739[a]	0.0
$ArNC^+$	**21**	$^1\Sigma^+$	−618.4615	−618.9358	*d*	−619.0448[a]	18.2[e]
CN^+		$^1\Sigma^+$	−91.6123	−91.9793	3.1	−92.0848 (−92.0496)[a]	

[a] At MP4(SDTQ)/6-311G(d,p). [b] Using MP2/6-31G(d,p) optimized geometries. [c] Including ZPE. [d] Not converged. [e] Without ZPE.

Scheme IV. Calculated Dissociation Energies (D_e and D_o, kcal/mol) at Several Theoretical Levels for $NgCN^+$ and $NgNC^+$ Molecules

	HF/6-31G(d,p)	MP2/6-31G(d,p)	MP4(SDTQ)/6-311G(2df,2pd)[b]		
	D_e	D_e	D_e	D_o	no.
$HeCN^+$ **16a** → He + CN^+	+40.4	−8.7	−17.9	−19.4	22
$HeCN^+$ **16b** → He + CN^+		+0.7	+0.9	+0.6	23
$HeNC^+$ **17a** → He + CN^+	−10.2				24
$HeNC^+$ **17b** → He + CN^+	+0.1	+0.8	+0.9	+0.4	25
$NeCN^+$ **18** → Ne + CN^+	+33.4	+6.8	+3.6	+2.0	26
$NeNC^+$ **19** → Ne + CN^+	+1.0	+5.8	+3.6	+2.2	27
$ArCN^+$ **20** → Ar + CN^+	+91.8	+50.8	+35.7[a]	+34.6[a]	28
$ArNC^+$ **21** → Ar + CN^+	+47.3	+22.9	+17.5[a]		29

[a] At MP4/6-311G(d,p)//MP2/6-31G(d,p). [b] Using geometries optimized at MP2/6-31G(d,p).

$^1\Delta$ state,[41] which has to be considered when assessing the thermodynamic stability of the $NgCCH^+$ ions. In any case, the reduced stability of the Ne compound is clearly reflected by these data.

Two of the three $NgCCH^+$ ions, namely **13** and **15**, possess covalent Ng,C bonds (see Table III). In case of the Ne compound **14**, the analysis of the energy density H_b reveals that the bond possesses only weak covalent character. Electrostatic interactions between Ne and $CCH^+(^1\Pi)$ should play a more important role, which is in line with the relatively low dissociation energy D_e of 7.1 kcal/mol (Scheme III).

We have also investigated the dissociation of **13** at the CASSCF level since ion **13** is one of the candidates for a chemical synthesis, and, therefore, its stability has to be verified beyond doubt. The CASSCF/6-31G(d,p) value of reaction 19b (15.0 kcal/mol) is in convincing agreement with the MP4(SDTQ)/6-311G(2df,2pd) result (15.4 kcal/mol, Scheme III). We conclude that the $HeCCH^+$ cation is likely to be observed in the decay process of TCCH. There should be an even greater chance to get the stable $ArCCH^+$ cation, while observation of the neon compound is less likely.

3.4. $NgCN^+$ and $NgNC^+$ Cations. The interaction energies between He and the isoelectronic eight-valence electron cations CO^{2+}, CF^{3+}, and CNe^{4+} have been reported in a recent theoretical study by Radom and co-workers.[42] $HeCO^{2+}$ ($^1\Sigma^+$) was calculated with a He,C equilibrium distance of 1.115 Å and a dissociation energy D_e into He + $CO^{2+}(^1\Sigma^+)$ of 45.8 kcal/mol. Also for $HeCF^{3+}$ ($^2\Sigma^+$) a rather short He,C distance of 1.148 Å was predicted. Even $HeCNe^{4+}$ was calculated at MP2/6-31G(d,p) with a short He,C distance of 1.170 Å. At the higher MP3/6-311G(d,p) level, $HeCNe^{4+}$ is not a minimum energy structure but dissociates into HeC^{3+} + Ne^+.[42]

CN^+ is the singly charged analogue of the multiply charged CX^{n+} series (X = O, F, Ne). The interaction energy between He and $CN^+(^1\Sigma^+)$ can be expected to be lower than between He and CO^{2+} (45.8 kcal/mol)[42] because the orbital energy of the $3\sigma_g$ LUMO (Figure 6) is higher in the singly charged cation. $NgCN^+$ is also isoelectronic with $NgCCH^+$. However, the lowest singlet state of CN^+ possesses $^1\Sigma^+$ symmetry,[43] while in the case of CCH^+ the $^1\Sigma^+$ state is an excited state.[41]

Figure 9a shows a perspective drawing of the calculated Laplace concentration of $CN^+(^1\Sigma^+)$. There is a σ hole at the C atom, which is not as deep as the σ hole at the terminal C atom of $HCC^+(^1\Sigma^+)$ shown in Figure 9b, but it is much deeper than the σ hole at the N atom of CN^+. The different shape of the two holes simply reflects the fact that the $3\sigma_g$ LUMO of CN^+ has a larger amplitude at the C atom. The CN^+ ion is an electron acceptor that pulls electrons into its valence shell holes both at the C and the N atom. From the Laplace concentration shown in Figure 9a it is clear that the electron acceptor ability of $CN^+(^1\Sigma^+)$ is lower than that of $CCH^+(^1\Sigma^+)$. Binding at the C atom should be stronger than at the N atom.

Both $HeCN^+$ and $NeCN^+$ have been investigated at the HF level of theory with various basis sets by Wilson and Green.[44] For $HeCN^+$, these authors predicted a linear geometry (distance He,C, 1.10–1.17 Å; C,N, 1.13–1.16 Å) and D_e values between 35 and 46 kcal/mol for He dissociation. In the case of $NeCN^+$ (Ne,C, 1.593 Å, D_e = 13.8 kcal/mol) only small basis set calculations could be carried out, but the authors concluded from their results that the D_e value for Ne dissociation should become similar to that of $HeCN^+$ with larger basis sets.[44]

We have optimized the geometries of $HeCN^+$ (**16**), $NeCN^+$ (**18**), and $ArCN^+$ (**20**) and the isomeric structures $HeNC^+$ (**17**), $NeNC^+$ (**19**), and $ArNC^+$ (**21**) at the HF/6-31G(d,p) and MP2/6-31G(d,p) level of theory. The calculated energies are shown in Table VI, and the optimized geometries are exhibited in Chart IV. In Scheme IV we show the theoretically predicted dissociation energies. In agreement with the predictions made by Wilson and Green,[44] $HeCN^+$ and $NeCN^+$ are calculated at the Hartree–Fock level with rather short Ng,C distances and rather large D_e values (40.4 kcal/mol (He) and 33.4 kcal/mol

(40) The $^2\Pi_u$ state is the lowest lying doublet state of CC^+ which has a $^4\Sigma^-_g$ ground state: Petrongolo, C.; Bruna, P.; Peyerimhoff, S. D.; Buenker, R. J. *J. Chem. Phys.* **1981**, *74*, 4594.

(41) Koch, W.; Frenking, G. *J. Chem. Phys.* in press.

(42) (a) Wong, M. W.; Nobes, R. H.; Radom, L. *Rapid Commun. Mass Spectrom.* **1987**, *1*, 3. (b) Radom, L.; Gill, P. M. W.; Wong, M. W.; Nobes, R. H. *Pure Appl. Chem.* **1988**, *60*, 183.

(43) Huber, K. P.; Herzberg, G. *Molecular Spectra and Molecular Structure. IV. Constants of Diatomic Molecules*; Van Nostrand Reinhold: New York, 1979.

(44) Wilson, S.; Green, S. *J. Chem. Phys.* **1980**, *73*, 419.

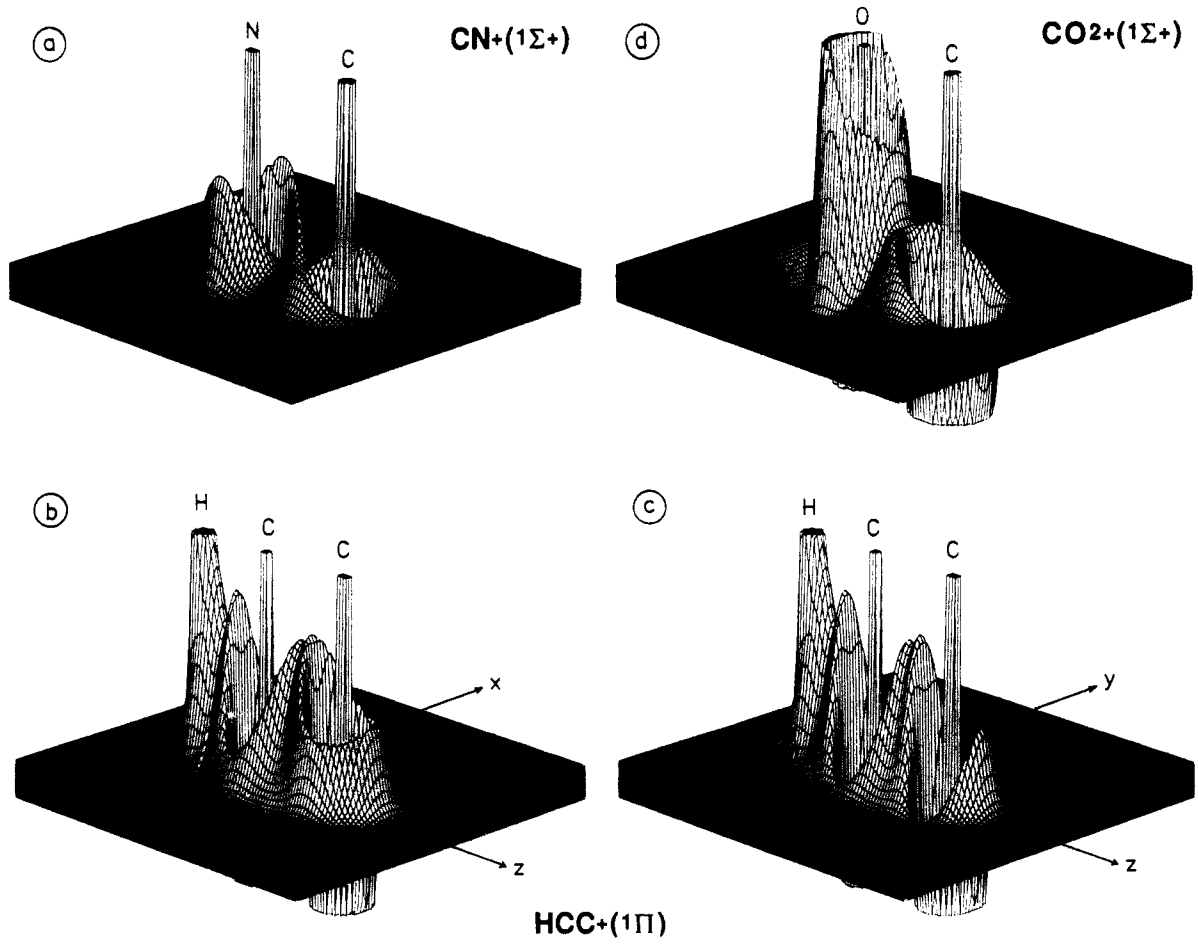

Figure 9. Perspective drawings of the HF/6-31G(d,p) Laplace concentration, $-\nabla^2\rho(r)$, of (a) $CN^+(^1\Sigma^+)$ shown from the side of the carbon atom, $HCC^+(^1\Pi)$ shown (b) in the plane with the two paired π-electrons and (c) shown in the plane with the unpaired π-electron, and (d) $CO^{2+}(^1\Sigma^+)$. Inner shell and valence shell concentrations are indicated. Note that the function value is cut off above and below predetermined values to improve the representation.

Chart IV. Optimized Geometries of $NgCN^+$ and $NgNC^+$ Structures and CN^+ at MP2/6-31G(d,p) (HF/6-31G(d,p))[a]

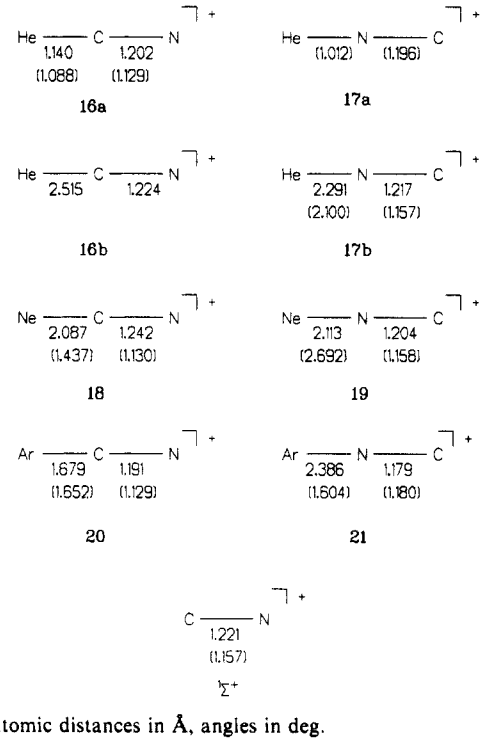

[a] Interatomic distances in Å, angles in deg.

(Ne)). For $ArCN^+$, even stronger Ar,C interactions are predicted at HF/6-31G(d,p) yielding D_e = 91.8 kcal/mol (Scheme IV). The $NgNC^+$ isomers are much less stable. For $HeNC^+$, two genuine minima on the HF/6-31G(d,p) potential energy surface were found (only positive eigenvalues of the diagonalized force-constant matrix), i.e., **17a** with a very short He,N distance of 1.012 Å and **17b** with a much longer He,N value of 2.100 Å (Chart IV). $HeNC^+$ (**17b**) and $NeNC^+$ (**19**) are predicted at the HF/6-31G(d,p) level to be weakly bound van der Waals (vdW) complexes with D_e = 0.1 kcal/mol (**17b**) and D_e = 1.0 kcal/mol (**19**). $ArNC^+$ (**21**), however, is calculated with a significant Ar,N stabilization energy (D_e = 47.3 kcal/mol).

Inclusion of correlation corrections leads to very different results. HeNC (**17a**) is not a minimum anymore at MP2/6-31G(d,p). Two genuine minima **16a** and **16b** are found for $HeCN^+$ at the MP2/31G(d,p) level. Similar to the Hartree–Fock results for $HeNC^+$, one structure (**16a**) has a rather short He,C distance (1.140 Å), while for the other form (**16b**) the He,C value is very large (2.515 Å). Clearly, the geometry of **16a** point toward covalent He,C bonding, while the optimized He,C distance in **16b** indicates a vdW complex.

This interpretation is confirmed by the analysis of electron and energy density distribution, which indicates covalent He,C bonding for **16a** and electrostatic He,C interactions for **16b**. But despite its covalent He,C bond, **16a** is not a stable molecule: Dissociation into He and $CN^+(^1\Sigma^+)$ is exoenergetic by 8.7 kcal/mol (MP2/6-31G(d,p)) and 17.9 kcal/mol (MP4/6-311G(2df,2pd), Scheme IV). The van der Waals complex **16b** is 9.4 and 18.8 kcal/mol lower in energy than **16a** at the MP2 and MP4 levels of theory, respectively. Complex **16b** itself is stable by a marginal energy of D_e = 0.9 kcal/mol with regard to dissociation into He and $CN^+(^1\Sigma^+)$. This value is reduced to D_0 = 0.6 kcal/mol when correlation corrections are considered (Scheme IV).

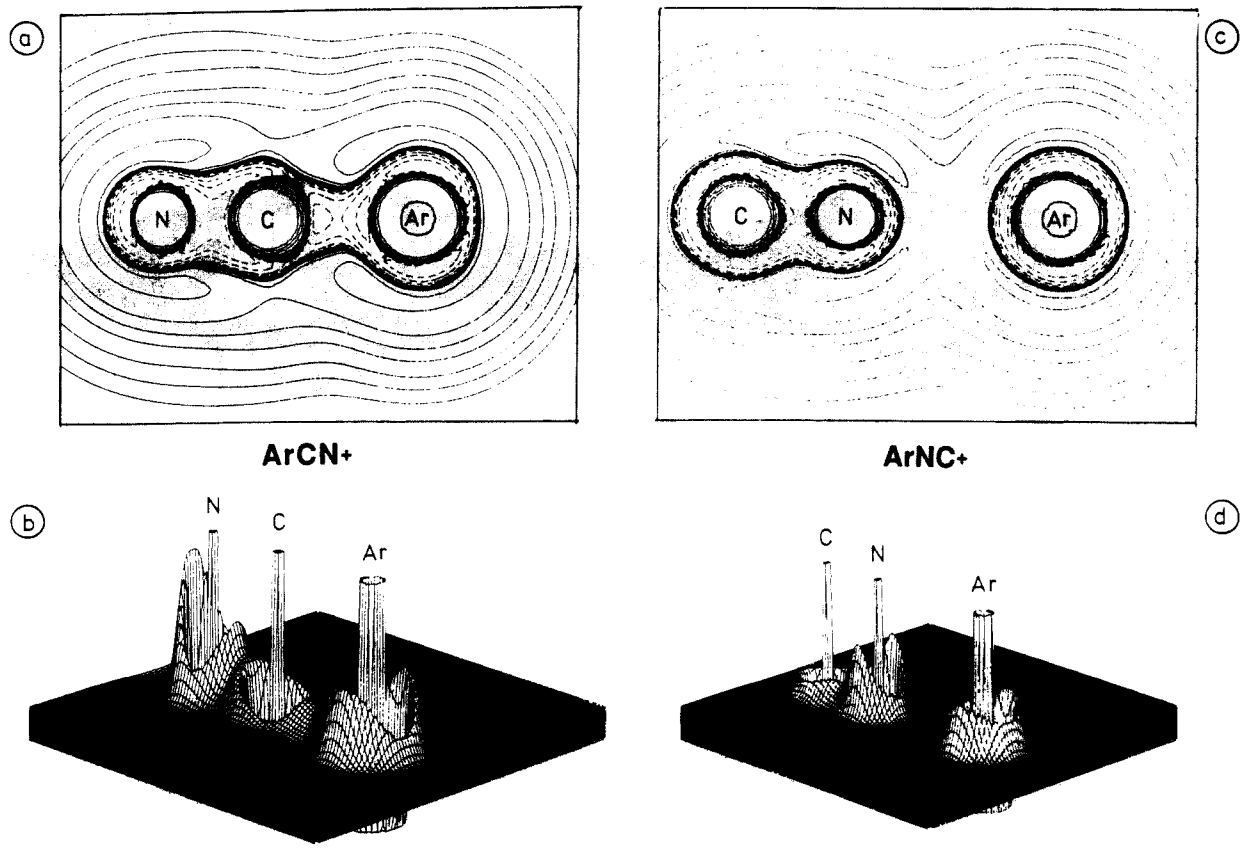

Figure 10. Contour line diagrams and perspective drawings of the HF/6-31G(d) Laplace concentration, $-\nabla^2\rho(r)$, of (a,b) $ArCN^+$ and (c,d) $ArNC^+$. In the contour line diagrams inner shell concentrations are no longer shown. In the perspective drawings, the function value is cut off above and below predetermined values to improve the representation.

Since these data suggest that **16a** is a spurious minima due to artifacts of method and basis set, we have investigated structure **16a** also at the CASSCF/6-31G(d,p) level of theory starting with the MP2/6-31G(d,p) geometry. In the course of the optimization procedure, the He,C distance became much longer ($r_{He,C} > 3$ Å) which indicates that **16a** is not a minimum at CASSCF/6-31G-(d,p). Hence, both isomeric forms $HeCN^+$ and $HeNC^+$ are moderately stable ($D_e < 1$ kcal/mol, Scheme IV) van der Waals complexes with rather long He,C and He,N interatomic distances, respectively. The same is also true for the two cations $NeCN^+$ (**18**) and $NeNC^+$ (**19**). The MP4 results (Scheme IV) suggest interaction energies of 3.6 kcal/mol between Ne and $CN^+(^1\Sigma^+)$ leading to a Ne,C distance of 2.09 Å in **18** and to a Ne,N distance of 2.11 Å in **19** (Chart IV). The properties of $\rho(r)$ and $H(r)$ indicate weak dipole-induced dipole interactions (Table III).

Contrary to $HeCN^+$ (**16**) and $NeCN^+$ (**18**), $ArCN^+$ (**20**) is a covalently bound stable noble gas ion (Table V). This is in line with the enhanced donor ability of Ar and the distinct acceptor ability of $CN^+(^1\Sigma^+)$ at its carbon end. Figure 10, which contains contour line diagrams and perspective drawings of calculated Laplace concentrations of the two possible $ArCN^+(^1\Sigma^+)$ ions **20** (Figure 10 (parts a and b)) and **21** (Figure 10 (parts c and d)), reveals pronounced $3p\sigma$ donation of the Ar atom and concentration of negative charge in the Ar,C bonding region. Electron donation from Ar to $CN^+(^1\Sigma^+)$ leads to a reorganization of electronic structure in the CN part of compound **20**, which is nicely illustrated by the perspective drawings of $-\nabla^2\pi(r)$ in Figure 9a ($CN^+(^1\Sigma^+)$) and Figure 10b.

The calculated electronic structure is completely different in ion $ArNC^+$ (**21**) as can be seen from Figures 10 (parts c and d). Obviously, there are now just electrostatic interactions between N and the noble gas atom in line with what has been found for $HeNC^+$ (**17**) and $NeNC^+$ (**19**). There is no concentration of negative charge in the region between Ar and N (Figure 10d), and the electronic structure of the $CN^+(^1\Sigma^+)$ ion seems to be hardly changed by the Ar atom (compare Figures 10d and 9a). This result clearly demonstrates that the σ hole at the N atom is too small to make $CN^+(^1\Sigma^+)$ an ambident noble gas acceptor with equal strength at the C and N end.

The dissociation energies D_e for **20** and **21** are 35.7 and 17.5 kcal/mol, respectively (Scheme IV). Again, the D_e value for **20** confirms the larger donor ability of Ar and the lower $p(\pi)$–$p(\pi)$ electron repulsion in Ar containing compounds with multiple bonds. The D_e value for **21** is relatively large in view of the electrostatic nature of the interactions. However, previous investigations of ArX^+ ions have shown that ion-induced dipole forces can lead to as much as 25 kcal/mol attraction between Ar and ions such N^+.[7] Our calculations show that despite the fact that CN^+ is isoelectronic with CC^+, of the six possible $NgCN^+$ and $NgNC^+$ systems, only $ArCN^+$ represents a covalently bonded stable ion.

4. Summary and Chemical Relevance

The helium, neon, and argon dications Ng_2C^{2+} have ($^1A_1$) singlet ground states and significantly stronger bound ($^3B_1$) excited states. He_2C^{2+} ($^1A_1$) is stable toward dissociation into the lowest lying atomic products $C^{2+}(^1S)$ + 2He. The $^3B_1$ state of He_2C^{2+} and the $^1A_1$ and $^3B_1$ state of Ne_2C^{2+} and Ar_2C^{2+} dissociate into the atomic products $Ng^+ + Ng + C^+(^2P)$. The charge separation reaction is energetically nearly balanced for ($^1A_1$) Ne_2C^{2+} but exothermic for the other species. The electronic structure and binding features are rationalized by invoking donor–acceptor interactions between Ng and C^{2+}. The ^3P state of C^{2+} is a much better electron acceptor than the ^1S state, which becomes evident by the analysis of the respective electron density distribution. Frontier orbital interactions are responsible for the stronger bonds in the triplet than in the singlet state. The attractive interactions increase for the singlet and triplet state with the order $He_2C^{2+} < Ne_2C^{2+} < Ar_2C^{2+}$ with the triplet state always being stronger bound. The increase in interaction energy in Ng_2C^{2+} is larger when going from Ne to Ar than from He to Ne. There is also an increase in binding interactions between Ng and X^{2+} (X = C,

N, O) for the three noble gas elements with the order $Ng_2C^{2+} < Ng_2N^{2+} < Ng_2O^{2+}$, if the ground states of the dications are compared. In spite of the increase in binding energy, the Ng_2N^{2+} and Ng_2O^{2+} ions are thermodynamically unstable in the respective charge separation reactions.

For $HeCCHe^{2+}$ and $NeCCNe^{2+}$, two different bound states are calculated as minima at the MP2(6-31G(d,p) level of theory, a linear form and an energetically lower lying trans-bent structure. Higher level calculations indicate that the trans-bent species are probably the only bound minima on the respective potential energy surface. The trans-bent form of $HeCCHe^{2+}$ has also been located at the CASSCF/6-31G(d,p) level of theory. In case of $ArCCAr^{2+}$, the geometries of the linear and bent forms differ very little and are energetically nearly degenerate. The energetically lower lying trans-bent geometries of $NgCCNg^{2+}$ are explained by the different electronic structure compared with neutral acetylene with use of MO correlation diagrams. $HeCCHe^{2+}$, $NeCCNe^{2+}$, and $ArCCAr^{2+}$ are thermodynamically stable toward breaking the Ng,C bond. Binding interactions between Ng and CC^{2+} in $NgCCNg^{2+}$ have comparable strength for Ng = He and Ng = Ne but are significantly stronger for Ng = Ar. $ArCCAr^{2+}$ is thermodynamically stable also toward breaking the C,C bond.

$HeCCH^+$, $NeCCH^+$, and $ArCCH^+$ have trans-bent geometries which are discussed in terms of interactions between Ng and CCH^+ ($^1\Pi$). The trans-bent geometries are found only when correlation energy is included in the calculation. $NeCCH^+$ is less stable toward loss of Ng (D_0 = 5.9 kcal/mol) than $HeCCH^+$ (D_0 = 12.5 kcal/mol), but $ArCCH^+$ has a significantly higher dissociation energy D_0 = 54.3 kcal/mol.

$HeCN^+$, $HeNC^+$, $NeCN^+$, and $NeNC^+$ are predicted to be weakly bound vdW complexes with dissociation energies $D_e < 4$ kcal/mol and rather long Ng,C and Ng,N equilibrium distances, respectively. In contrast, $ArCN^+$ and $ArNC^+$ have substantially higher dissociation energies D_e of 35.7 and 17.5 kcal/mol, respectively.[45]

The model of donor–acceptor interactions, which has been proven as very successful for helium compounds,[2] seems to be equally valid for the rationalization of Ne and Ar molecules. Generally, there is an increase in Ng,X binding interactions with He,X < Ne,X < Ar,X. In some cases, the presence of p–π repulsive interactions causes lower stabilization energies for Ne,X than for He,X. Ar,X molecules exhibit substantially higher binding energies than He,X and Ne,X molecules.

The essential results of our previous[2,3,6-8] and present ab initio investigations on He-, Ne-, and Ar-containing compounds can be summarized as follows.

(a) Our results provide sufficient theoretical evidence that supports the existence of stable molecules containing He, Ne, or Ar. These noble gas elements have been considered until recently to be completely inert.

(b) Both charged and neutral[2,3] He, Ne, and Ar compounds are predicted on the basis of correlation corrected ab initio calculations. The various classes of possible Ng compounds are listed in Table VII.

(c) Structure and stability of Ng compounds are best understood in terms of donor–acceptor interactions between the weak donor Ng and a strong acceptor X.

(d) In order to be a strong acceptor of Ng electrons, X has to possess σ concentration holes in its valence shell, i.e., low-lying unoccupied σ orbitals.

(e) σ Holes are more important for the Ng acceptor ability of X than positive charges or a large electronegativity of X. That is the reason why singly charged or even neutral Ng compounds[2,3] are predicted. On the basis of the donor–acceptor model we predict that long-searched compounds such as HeO[46] or HeF_2[47] do not exist.

(f) He, Ne, and Ar can form semipolar covalent bonds with the acceptor X. Also possible are electrostatic bonds and the formation of exceptionally stable van der Waals complexes.

On the basis of findings (a)–(f) we suggest the following experiments to be carried out in order to confirm the existence of He-, Ne-, or Ar-containing compounds.

(A) Mass spectroscopic studies of molecular ions produced by electric discharges in a Ng atmosphere. This has successfully been done by Young and Coggiola,[48] who detected HeC^+ with graphite as the cathode in helium atmosphere. A different choice of the cathode material and/or the atmospheric condition could provide a source of noble gas molecular ions which can be used for gas-phase experiments. This is important for the study of potential interstellar ions containing He, which is the second most abundant element in outer space.[49] Since spectroscopic constants of small molecules can be predicted quite accurately by quantum chemical calculations, theory may help to identify such species.

(B) Investigation of the decay products of tritiated compounds. β Decay of tritium yields He^+, besides a neutrino particle. Spurious amounts of HeX^+ cations such as $HeCH_3^+$ have been detected already in the 60s[50] by mass spectroscopic studies, although these species are theoretically predicted to be bound by less than 1 kcal/mol.[51] Considering these results, $HeCCH^+$ should easily be observed and could be used for molecular beam experiments. Very recently, Hanack and co-workers[52] used tritiated acetylene derivatives and reported the first evidence for the existence of an acetylene cation $R–CC^+$ in solution. If the same experiment would be performed in the gas phase, it should be possible to detect the precursor ion $R–CCHe^+$.

Table VII. Potentially Stable or Metastable He-, Ne-, and Ar-Containing Compounds[b]

thermodynamically stable molecule	ΔE_0	metastable
	A. Dications	
$He_2C^{2+}(^1A_1)$	13.6	$He_2C^{2+}(^3B_1)$; $He_2N^{2+}(^2B_1)$; $He_2O^{2+}(^1A_1)$; $Ne_2C^{2+}(^1A_1)$; $Ne_2C^{2+}(^3B_1)$; $Ne_2N^{2+}(^2B_1)$; $Ne_2O^{2+}(^1A_1)$; $Ar_2C^{2+}(^1A_1)$; $Ar_2C^{2+}(^3B_1)$; $Ar_2N^{2+}(^2B_1)$; $Ar_2O^{2+}(^1A_1)$
$ArCCAr^{2+}$	9.4	$HeCCHe^{2+}$; $NeCCNe^{2+}$
	B. Monocations	
$HeCCH^+$	12.5	
$NeCCH^+$	5.9	
$ArCCH^+$	54.3	
$ArCN^+$	34.6	
$ArNC^+$	17.5 (ΔE_e)	
	C. Neutral Compounds	
HeBeO	3.1[a]	
NeBeO	2.2[a]	
ArBeO	7.0[a]	

[a] Taken from ref 3. [b] For the thermodynamically stable molecules, the calculated reaction energy ΔE_0 (in kcal/mol) for the least endothermic reaction is given.

(45) One referee pointed out, that the basis set superposition error (BSSE) may significantly influence the reliability of our theoretically predicted dissociation energies. We have studied this effect in previous investigations[6-8] and found that, at MP4/6-311G(2df,2pd), typical errors due to BSSE are 0.1–1.0 kcal/mol for He compounds, 1.0–4.0 kcal/mol for neon compounds, and 1.0–2.0 kcal/mol for Ar compounds. The possible small error introduced by BSSE does not influence the conclusions drawn in this study.

(46) (a) Allen, L. C.; Lesk, A. M.; Erdahl, R. M. *J. Am. Chem. Soc.* **1966**, *88*, 615. (b) Fereday, R. J.; Sinha, S. P. *J. Chim. Phys.* **1977**, *74*, 87. (c) Masse, J. L.; Masse-Baerlocher, M. J. *J. Chim. Phys.* **1967**, *64*, 417.

(47) (a) Allen, L. C.; Erdahl, R. M.; Whitten, J. L. *J. Am. Chem. Soc.* **1965**, *87*, 3769. (b) Ferreira, R. *Chem. Phys. Lett.* **1968**, *2*, 233. (c) Noble, P. N.; Kortzeborn, R. N. *J. Chem. Phys.* **1970**, *52*, 5375.

(48) Young, S. E.; Coggiola, M. J. *Int. J. Mass Spectrom. Ion Proc.* **1986**, *74*, 137.

(49) Duley, W. W.; Williams, D. A. *Interstellar Chemistry*; Academic Press: London, 1984.

(50) (a) Snell, A. H.; Pleasonton, F. *J. Phys. Chem.* **1958**, *62*, 1377. (b) Cacae, F. *Adv. Phys. Chem.* **1970**, *8*, 79. (c) Evans, E. A. *Tritium and Its Compounds*; Van Nostrand: London, 1966.

(51) Wong, M. W.; Nobes, R. H.; Radom, L. *J. Chem. Soc., Chem. Commun.* **1987**, 233.

(52) Angelini, G.; Hanack, M.; Vermehren, J.; Speranza, M. *J. Am. Chem. Soc.* **1988**, *110*, 1298.

(C) Salt compounds of ArF^+: The bond energy of ArF^+ in its $^1\Sigma^+$ ground state has recently been predicted by us as 49 ± 3 kcal/mol.[8] It was estimated that this should be sufficient to form stable salts such as $ArFAuF_6$ or $ArFSbF_6$.[8] This might be achieved by electric oxidation of F_2 in the presence of AuF_5 and Ar.

(D) NgBeO compounds, which have been predicted[2,3] to be stable for Ng = He, Ne, and Ar, might be detected by pyrolysis of polymeric BeO and trapping the monomeric BeO in fluid Ng. Another approach might be laser desorption of monomeric BeO from polymeric BeO in a Ng atmosphere.[54]

(E) Perutz and Turner[53] have shown that spectroscopic interactions of Ar with metal pentacarbonyls at 20 K can yield a substantial frequency shift which can only be explained by assuming that Ar occupies the sixth ligand position at $Cr(CO)_5$, $Mo(CO)_5$, and $W(CO)_5$. They conclude that "these stereospecific interactions are tantamount to the formation of a chemical bond".[53] While these observations have been made by accident, a systematic search for better acceptor species could result in even more stable transition metal–argon complexes.

Our suggestions for appropriate experiments are based on traditional laboratory techniques, but other ways will certainly be found by the inventive chemist. The chemistry of the light noble gases is a new field which is ideally suited for a combined theoretical/experimental approach.

Acknowledgment. Stimulating discussions with Prof. Christian K. Jørgensen, Dr. Jürgen Gauss, and Prof. Joel F. Liebmann are gratefully acknowledged. Part of this research has been supported by a grant of computer time from the San Diego Supercomputer Center. G.F. and D.C. thank the Deutsche Forschungsgemeinschaft and the Fonds der Chemischen Industrie for financial support. Calculations in Götegorg have been carried out using the CRAY XMP 48 of the NSC, Linköping, Sweden. W.K. thanks the IBM Düsseldorf computing center for providing computer time.

Supplementary Material Available: Table of calculated harmonic vibrational frequencies for **1–20** (2 pages). Ordering information is given on any current masthead page.

(53) Perutz, R. N.; Turner, J. J. *J. Am. Chem. Soc.* **1975**, *97*, 4791.
(54) This has been suggested by M. Devries.

NMR Studies of Cobalt(II)-Substituted Derivatives of Bovine Copper–Zinc Superoxide Dismutase. Effects of pH, Phosphate, and Metal Migration

Li-June Ming and Joan Selverstone Valentine*

Contribution from the Department of Chemistry and Biochemistry, University of California, Los Angeles, Los Angeles, California 90024. *Received July 17, 1989*

Abstract: The effects of changing pH and phosphate concentration on a number of Co^{2+}-substituted derivatives of bovine copper–zinc superoxide dismutase (Cu_2Zn_2SOD) have been studied by means of electronic spectroscopy, isotropically shifted ^1H NMR spectroscopy, and NMR relaxation. For the derivative E_2Co_2SOD, a pH-dependent Co^{2+} migration from the zinc site to the empty copper site was observed, forming subunits containing Co^{2+} in both metal binding sites. The presence of phosphate was observed to faciliate the cobalt migration process, presumably due to the fact that the anion causes an enhancement of Co^{2+} binding to the copper site. Some related studies of pH-dependent effects in the presence and absence of phosphate were carried out on Co_2Co_2SOD and Co_2Zn_2SOD, derivatives with Co^{2+} in the copper site, and on $Cu^I_2Co_2SOD$ and $Ag^I_2Co_2SOD$, derivatives with Co^{2+} in the zinc site. Phosphate had earlier been reported to have a strong influence on the geometry of Co^{2+} in the copper site under neutral pH conditions. We found, however, that this effect was not present under highly alkaline conditions where no influence of phosphate was observed. We also found that pH was an important factor in determining whether or not the imidazolate bridge was present between the two metal ions in each subunit in the derivatives with Co^{2+} bound in the copper site. Under high pH conditions, the bridging imidazolate was present in the derivative $Ag^I_2Co_2SOD$, but not in the derivative $Cu^I_2Co_2SOD$ (an analogue of reduced native SOD), which retained its metal binding configuration, at least in the zinc site, over a wide range of pH.

Bovine copper–zinc superoxide dismutase (Cu_2Zn_2SOD)[1] is a dimeric metalloenzyme containing a Cu^{2+} ion and a Zn^{2+} ion in each of its identical subunits.[2] The two metal ions are bound in close proximity, 6.3 Å apart, and are bridged by the imidazolate ring of histidine-61.[2] The copper binding site is known to be the active site for the disproportionation of superoxide anion to dioxygen and hydrogen peroxide ($2O_2^- + 2H^+ \rightarrow O_2 + H_2O_2$). A variety of metal ions, including Co^{2+}, Cu^{2+}, Zn^{2+}, Cd^{2+}, Ag^+, and Hg^{2+}, have been shown to substitute for the native metal ions, Cu^{2+} and Zn^{2+}, in the enzyme, but only derivatives with Cu^{2+} in the copper site have substantial SOD activity.[2] Recently, some Ni^{2+}-substituted derivatives have also been prepared and char-

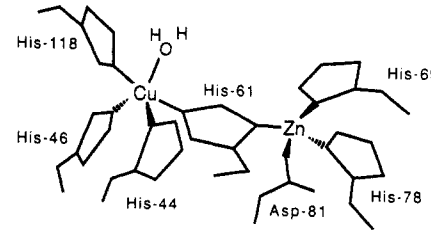

(1) Abbreviations: SOD, superoxide dismutase; $M_2M'_2SOD$, M- and M′-substituted SOD with M in the copper site and M′ in the zinc site (M and M′ are divalent metal ions unless otherwise noted), and an E represents an empty site; NMR, nuclear magnetic resonance; EPR, electron paramagnetic resonance; DEFT, driven equilibrium Fourier transform; FID, free induction decay; HEPES, 4-(2-Hydroxyethyl)-1-piperazineethanesulfonic acid; TMS, trimethylsilane.
(2) For a general reference, see: Valentine, J. S.; Pantoliano, M. W. In *Copper Proteins*; Spiro, T. G., Ed.; Wiley: New York, 1981; Vol. 3, Chapter 8.

0002-7863/90/1512-4256$02.50/0